Few-Shot Causal Representation Learning for Out-of-Distribution Generalization on Heterogeneous Graphs

Pengfei Ding, Yan Wang, Senior Member, IEEE, Guanfeng Liu, Member, IEEE, and Nan Wang

Abstract—Heterogeneous graph few-shot learning (HGFL) has been developed to address the label sparsity issue in heterogeneous graphs (HGs), which consist of various types of nodes and edges. The core concept of HGFL is to extract generalized knowledge from rich-labeled classes in a source HG, transfer this knowledge to a target HG to facilitate learning new classes with few-labeled training data, and finally make predictions on unlabeled testing data. Existing methods typically assume that the source HG, training data, and testing data all share the same distribution. However, in practice, distribution shifts among these three types of data are inevitable due to (1) the limited availability of the source HG that matches the target HG distribution, and (2) the unpredictable data generation mechanism of the target HG. Such distribution shifts can degrade the performance of existing methods, leading to a novel problem of out-ofdistribution (OOD) generalization in HGFL. To address this challenging problem, we propose a Causal OOD Heterogeneous graph Few-shot learning model, namely COHF. In COHF, we first characterize distribution shifts in HGs with a structural causal model, where an invariance principle can be explored for OOD generalization. Then, following this invariance principle, we propose a new variational autoencoder-based heterogeneous graph neural network to mitigate the impact of distribution shifts. Finally, by integrating this network with a novel metalearning framework, COHF effectively transfers knowledge to the target HG to predict new classes with few-labeled data. Extensive experiments on seven real-world datasets have demonstrated the superior performance of COHF over the state-of-the-art methods.

I. INTRODUCTION

Heterogeneous graphs (HGs), consisting of various types of nodes and edges, have been widely used to model complex real-world systems [1]. Consider the HGs in Fig. 1, which model movie-related social networks. These HGs include multiple types of nodes (e.g., user and actor) and edges (e.g., user U_1 "likes" actor A_5 , director D_4 "shoots" movie M_{11}). The variety of node and edge types necessitates substantial labeled data to learn effective representations on HGs for various downstream tasks (e.g., node classification) [2]. In real-world scenarios, label sparsity is a common issue because labeling nodes/edges/subgraphs with specific classes (e.g., labeling movie nodes as musical or romantic) demands considerable expertise and resources [3]. To address this issue, heterogeneous graph few-shot learning (HGFL) has been developed, which aims to extract generalized knowledge (a.k.a.,

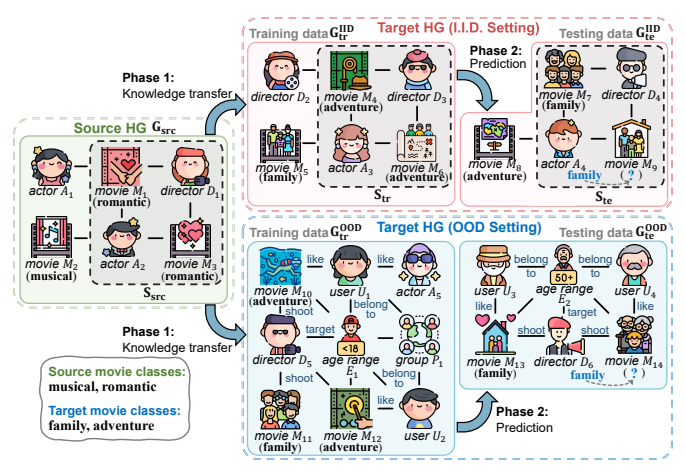


Fig. 1. Heterogeneous graph few-shot scenarios in I.I.D. and OOD settings.

meta-knowledge) from rich-labeled classes in a source HG, and then transfer this meta-knowledge to the target HG to facilitate learning new classes with few-labeled data. Typical forms of meta-knowledge include node informativeness [4], heterogeneous information from shared node types [5], and semantic information of specific graph structures [6].

It is worth mentioning that existing HGFL studies generally assume that data is independently and identically distributed (I.I.D.). This assumption posits that the rich-labeled data in the source HG, few-labeled training data in the target HG, and unlabeled testing data are all considered to come from the same distribution. The I.I.D. assumption simplifies both the problem modeling and the theoretical analysis, thereby easing the extraction of generalized knowledge and the design of HGFL models [5], [7]. For instance, in Fig. 1, under the I.I.D. setting, the source HG G_{src} , training data G_{tr}^{IID} , and testing data G_{te}^{IID} exhibit similar subgraphs S_{src} , S_{tr} and S_{te} , respectively. These subgraphs share a common circular structure that connects nodes of <movie, director, movie, actor> in a cyclical pattern. Therefore, the general information regarding this circular structure can serve as meta-knowledge to facilitate prediction in G_{te}^{IID} . Specifically, in S_{src} of G_{src} , the fact that both movie M_1 and M_3 belong to the same class (romantic) reveals knowledge that movie nodes within the circular structure tend to have similar classes. The generalizability of this knowledge can be validated in S_{tr} of G_{tr}^{IID} , where M_4 and M_6 are both adventure movies. Consequently, this generalized knowledge can be used in G_{te}^{IID} to predict the class of movie nodes in S_{te} , i.e., M_9 is likely to share the same class as M_7 (action).

P. Ding, Y. Wang, G. Liu and N. Wang are with the School of Computing, Macquarie University, Sydney NSW 2109, Australia. E-mail: pengfei.ding2@students.mq.edu.au, {guanfeng.liu, yan.wang}@mq.edu.au, nan.wang12@students.mq.edu.au.

However, in real-world scenarios, the I.I.D. assumption of existing studies is normally not satisfied. This is mainly because (1) the limited availability of the source HG that perfectly matches the target HG distribution [4], and (2) the unpredictable nature of data generation processes in the target HG [8]. As a result, distribution mismatches (a.k.a. distribution shifts) are inevitable between the source HG and the target HG, leading to complex out-of-distribution (OOD) environments in HGFL. As a new topic that remains unexplored in the existing literature, OOD environments in HGFL exhibit two unique characteristics as follows:

- 1. Multi-level Characteristic: Distribution shifts in HGFL can occur at three levels: feature-level (e.g., variations in node/edge features), topology-level (e.g., changes in graph size or other structural properties), and heterogeneity-level (e.g., discrepancies in node/edge types). These different levels of distribution shifts often occur simultaneously. For instance, in the OOD setting of Fig. 1, compared with the source HG G_{src} , the training data G_{tr}^{OOD} introduces new node types (e.g., user and group) and new edge types (e.g., "target" and "like"), leading to a heterogeneity-level shift between G_{src} and G_{tr}^{OOD} . Additionally, these new node and edge types contribute to a different graph structure and an increase in graph size, resulting in a topology-level shift between G_{src} and G_{tr}^{OOD} .
- **2. Phase-spanning Characteristic:** Distribution shifts in HGFL can occur in both the *knowledge transfer* phase and the *prediction* phase of the few-shot learning process. For example, in the OOD setting of Fig. 1, during the knowledge transfer phase, the introduction of new node and edge types in G_{tr}^{OOD} results in a heterogeneity-level shift between G_{src} and G_{tr}^{OOD} . In the prediction phase, the differences in age ranges (i.e., 'below 18' vs. 'over 50') between G_{tr}^{OOD} and G_{te}^{OOD} lead to variations in user node features, yielding a feature-level shift between nodes in these two graphs.

The multi-level and phase-spanning nature of OOD environments in HGFL not only undermines effective knowledge transfer from the source HG to the target HG, but also affects the prediction of testing data based on the features learned from training data. For instance, in Fig. 1, due to the topologylevel shift between G_{src} and G_{tr}^{OOD} , the knowledge of the circular structure S_{src} cannot be transferred to G_{tr}^{OOD} . Moreover, the feature-level shift between nodes in G_{tr}^{OOD} and G_{te}^{OOD} can lead to incorrect predictions for movie nodes in G_{le}^{OOD} . Therefore, it is crucial to investigate the consistency across source HG, training data, and testing data, which remains stable in contrast to distribution shifts. For instance, in Fig. 1, the knowledge that movie nodes connected to the same director node typically belong to the same class, can be inferred from G_{src} , e.g., movie M_1 and M_3 linked with director D_1 are classified as *romantic*. This knowledge can be further refined in the OOD setting: movie nodes connected to the same director node may share a class if they target the same user group, e.g., in G_{tr}^{OOD} , M_{10} and M_{12} directed by D_5 targeting user nodes 'under 18' fall into the same class (adventure). This pattern remains consistent in G_{te}^{OOD} , where M_{13} and M_{14} directed by D_6 targeting user nodes aged 'over 50' belong to the same class (family). This example illustrates the presence of consistency in OOD environments, and exploring such consistency is important for robust knowledge transfer and accurate predictions.

The above discussion reveals a novel problem of out-ofdistribution generalization on heterogeneous graph few-shot learning, which aims to handle distribution shifts not only between the source HG and the target HG, but also between the training and testing data in the target HG. To tackle this new problem, we have to face three key challenges as follows. CH1. How to figure out the invariance principle in HGs to enable OOD generalization in heterogeneous graph fewshot learning? The invariance principle implies that model predictions, which focus only on the causes of the label, can remain consistent to a range of distribution shifts [9], [10]. This principle forms the cornerstone of many studies that enable OOD generalization in regular Euclidean data (e.g., images) [11]. While recent efforts have extended this principle to non-Euclidean data and addressed distribution shifts in graphs, they primarily focus on homogeneous graphs with a single type of nodes and a single type of edges [12], [13]. However, exploring the invariance principle in heterogeneous graphs is non-trivial, because it requires extracting intricate semantics that remain unaffected by distribution shifts. Such semantics may comprise diverse node and edge types with complicated structural characteristics. Therefore, exploring a new invariance principle in HGs poses a significant challenge. CH2. How to achieve effective knowledge transfer from the source HG to the target HG in OOD environments? Most HGFL methods transfer knowledge through shared node types or common graph structures between the source HG and the target HG [5], [7]. However, distribution shifts in HGFL can introduce heterogeneity and structural variances between these HGs, potentially leading to ineffective knowledge transfer or even negative transfer [14]. Considering the multi-level nature of these distribution shifts, developing a novel knowledge transfer framework is a substantial and complex challenge. CH3. Given few-labeled data sampled from an OOD environment, how to effectively learn the class associated with these samples? Existing few-shot learning methods are primarily designed for I.I.D. environments. These methods aim to derive comprehensive class information from limited samples [15],

To address the above three challenges, we propose a novel <u>Causal QOD Heterogeneous graph Few-shot</u> learning model, called COHF. To address **CH1**, we construct a structural causal model (SCM) to analyze the cause-effect factors that influence the generation of node labels. Based on the SCM, we discover the invariance principle for OOD generalization in HGs: heterogeneous graph neural networks (HGNNs) remain invariant to distribution shifts by focusing only on environment-independent factors. To address **CH2**, we follow this principle and devise a new variational autoencoder-based HGNN module (VAE-HGNN). To mitigate the effects of distribution shifts, VAE-HGNN incorporates an encoder to inferring invariant factors from the source HG and includes

[16]. However, OOD environments demand a focus on aspects of class information that remain invariant with distribution

shifts, rather than attempting to capture all class information.

This poses the challenge of identifying invariant class infor-

mation with only a few labeled samples available.

a decoder that utilizes these invariant factors to predict labels in the target HG. To address **CH3**, we propose a novel meta-learning based module that transfers the knowledge of measuring the richness of invariant factors from the source HG to the target HG. This module evaluates the importance of few-labeled samples to derive robust class representations for prediction.

To the best of our knowledge, our work is the first to propose the novel problem of OOD generalization in heterogeneous graph few-shot learning and provide a solution for it. Our key contributions are as follows:

- We propose the COHF model, which performs causal modeling and inference to handle various distribution shifts in heterogeneous graph few-shot learning;
- We develop a novel heterogeneous graph neural network module that can extract invariant factors in HGs, and introduce a novel meta-learning module that can achieve effective knowledge transfer and robust predictive performance in OOD environments;
- We conduct extensive experiments on seven real-world datasets. The results demonstrate the superiority of our COHF model over the state-of-the-art methods.

II. RELATED WORK

A. Heterogeneous Graph Representation Learning

Heterogeneous graph representation learning aims to learn low-dimensional node embeddings for various network mining tasks. Recently, heterogeneous graph neural networks (HGNNs) have shown promising results in learning representations on HGs. HGNNs can be categorized into two main groups: type-based and meta-path based. Type-based HGNNs directly model various types of nodes and edges. For example, HetSANN [17] incorporates type-specific graph attention layers to aggregate local information, while Simple-HGN [18] adopts learnable edge type embeddings for edge attention. SlotGAT [19] develops a slot-based message passing mechanism to explore semantics in different node-type feature spaces. In contrast, meta-path based HGNNs focus on modeling meta-paths to extract hybrid semantics in HGs. For instance, HAN [20] employs a hierarchical attention mechanism to capture node-level importance between nodes and semantic-level importance of meta-paths. MAGNN [21] provides an advanced approach with several meta-path encoders to encode comprehensive information along meta-paths. GTN [22] can automatically learn meta-paths using graph transformation layers. However, these methods often assume the same distribution between training and testing data, which limits their generalizability to OOD environments in HGs.

B. Graph Few-shot Learning

Graph few-shot learning combines few-shot learning with GNNs to address label sparsity issues. Most existing studies focus on homogeneous graphs [2]. For example, Meta-GNN [23] combines GNNs with the MAML algorithm [15] for effective graph learner initialization. G-Meta [16] utilizes metagradients from local subgraphs to update network parameters.

Recent studies have extended few-shot learning to heterogeneous graphs. For instance, META-HIN [24] employs multiple Bi-LSTMs to capture information from various node types and integrates the HGNN with a meta-learning framework to address few-shot problems on a single HG. CrossHG-Meta [25] and HG-Meta [7] leverage shared meta-paths between source and target HGs to enhance generalizability. However, these methods overlook diverse distribution shifts in HGs and are ineffective in OOD environments, e.g., if there is a heterogeneity-level shift between the source HG and the target HG, these methods cannot be generalized to the target HG due to differences in node types or meta-paths. CGFL [4] addresses the cross-heterogeneity challenge by simplifying heterogeneous information into two general patterns for knowledge transfer. However, this approach still overlooks distribution shifts between training and testing data. Additionally, this simplification may lead to the loss of specific node type information, limiting the capability to capture invariant heterogeneous information in OOD environments.

C. OOD Generalization on Graphs

Some pioneering works [26], [27] have investigated whether models trained on small graphs can generalize effectively to larger ones [28]. Recently, researchers have extended OOD generalization methods, such as the invariance principle [29], to explore graph structures that are resilient to distribution shifts. For instance, DIR [30] divides a graph into causal and non-causal components using an edge threshold. CIGA [12] aims to maximize the agreement between the invariant portions of graphs with the same labels. CAL [31] uncovers causal patterns and mitigates the confounding effects of shortcuts. DisC [13] investigates learning causal substructures in scenarios with severe bias. However, most of these efforts focus on graph classification tasks in homogeneous graphs. Notably, there is a lack of research addressing more comprehensive graph distribution shifts in heterogeneous graphs.

D. Domain-Invariant Feature Learning

Domain-invariant feature learning aims to learn domaininvariant representations via deep learning models, so that the models trained on a labeled source domain can be transferred to a target domain without labeled samples (a.k.a., unsupervised domain adaption (UDA)). While numerous works have been designed for image and text data [32], [33], only a few methods have been proposed for graph data. For instance, UDA-GCN [34] achieves cross-domain node embedding by deceiving the domain discriminator. MuSDAC [35] focuses on heterogeneous graphs and utilizes multi-space alignment to enable domain adaptation across different semantic spaces. However, UDA methods assume that the target domain is entirely unlabeled. They primarily seek to minimize error in the source domain and bridge distribution gaps between domains through alignment techniques. In some cases, the performance of domain adaptation cannot be guaranteed [36].

III. PRELIMINARIES

Heterogeneous Graph. A heterogeneous graph is defined as $G = (\mathcal{V}, \mathcal{E}, \mathcal{S}_n, \mathcal{S}_e)$, where \mathcal{V} represents the set of nodes with a

TABLE I NOTATIONS USED IN THIS PAPER.

Notation	Explanation
\overline{G}	Heterogeneous graph
$\mathcal{V} \ \mathcal{E}$	Set of nodes
	Set of edges
$arphi(\cdot)$	Node type mapping function
Φ	Single node type
$egin{array}{c} \dot{\Phi} \\ \mathcal{S}_n \\ \mathcal{S}_e \end{array}$	Set of node types
\mathcal{S}_e	Set of edge types
$\tau = (\tau_{spt}, \tau_{qry})$	Single few-shot task
$p_{ heta}(\cdot)$	Distribution parameterized by θ
$q_\phi(\cdot)$	Variational distribution parameterized by ϕ
\mathbf{rel}^c	Set of common relations
\mathbf{rel}^u	Set of unique relations
a_{uv}	Connectivity between nodes u and v
A	Adjacency matrix
G_{s}	Subgraph structure around the target node
\mathbf{X}	Raw node features
$\mathbf{H}^{(l)}$	Hidden embedding of the <i>l</i> -th layer
\mathbf{h}_v	Hidden embedding of node v
\mathbf{W}	Weight matrix
α, γ	Normalized attention weight
$rsl(\cdot), rnl(\cdot)$	Richness score of structure-level and node-level
\mathbf{proto}_c	Prototype embedding of class c

node type mapping function $\varphi(v): \mathcal{V} \mapsto \mathcal{S}_n$, and \mathcal{E} denotes the set of edges with an edge type mapping function $\psi(e): \mathcal{E} \mapsto \mathcal{S}_e$. \mathcal{S}_n and \mathcal{S}_e represent the sets of node types and edge types, respectively. Each node $v \in \mathcal{V}$ or edge $e \in \mathcal{E}$ is associated with a specific type. Note that $|\mathcal{S}_n| + |\mathcal{S}_e| > 2$ for heterogeneous graphs. Table I summarizes frequently used notations in this paper for quick reference.

Problem Formulation. In this work, we focus on the problem of few-shot node classification in HGs under OOD environments. To mimic few-shot scenarios, we create two sets of few-shot tasks for the source HG and the target HG, named \mathcal{T}_{src} and \mathcal{T}_{tgt} respectively.

- **Input:** Source HG G_{src} with its task set \mathcal{T}_{src} . Target HG training data G_{tgt}^{tr} with its task set \mathcal{T}_{tgt} . The distribution $\Psi(G_{src}) \neq \Psi(G_{tgt}^{tr})$.
- Output: A model with good generalization ability to accurately predict the labels of nodes in the target HG testing data G_{tot}^{te} , where the distribution $\Psi(G_{tot}^{tr}) \neq \Psi(G_{tot}^{te})$.

Few-shot Task Construction. The set of m few-shot tasks on an HG, denoted as $\mathcal{T} = \{\tau_1, \tau_2, \dots, \tau_m\}$, is constructed as follows: Under the N-way K-shot setting, each task $\tau = (\tau_{spt}, \tau_{qry})$ is composed by first selecting N different classes $C_{\tau} = \{c_1, c_2, \dots, c_N\}$ from the label space C. Then, the support set $\tau_{spt} = \{\tau_{c_1}, \tau_{c_2}, \dots, \tau_{c_N}\}$ is formed by sampling K labeled nodes from each class, *i.e.*, $\tau_{c_i} = \{(v_1, c_i), (v_2, c_i), \dots, (v_K, c_i)\}$. The query set $\tau_{qry} = \{\tilde{\tau}_{c_1}, \tilde{\tau}_{c_2}, \dots, \tilde{\tau}_{c_N}\}$ is created using the remaining nodes from each class, where $\tilde{\tau}_{c_i} = \{(\tilde{v}_1, c_i), (\tilde{v}_2, c_i), \dots, (\tilde{v}_K, c_i)\}$.

For each task on the target HG ($\tau \in \mathcal{T}_{tgt}$), the support set and query set are sampled from the training data G_{tgt}^{tr} and the testing data G_{tgt}^{te} , respectively. After sufficient training iterations over all few-shot tasks in the source HG (\mathcal{T}_{src}), the obtained model is expected to solve each few-shot task in the target HG (\mathcal{T}_{tgt}) by performing N-way classification in G_{tgt}^{te} , utilizing only K labeled examples per class from G_{tgt}^{tr} .

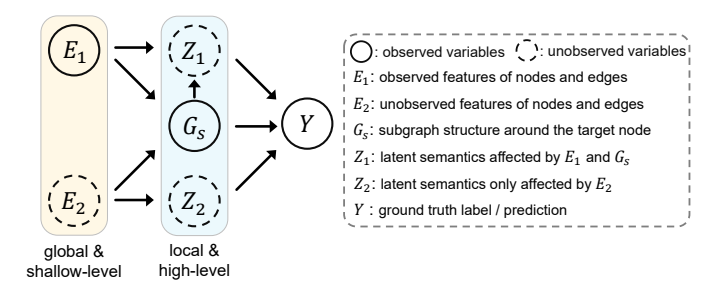


Fig. 2. Structure causal model (SCM) for node label generation in HGs.

IV. INVARIANCE PRINCIPLE FOR OOD GENERALIZATION ON HETEROGENEOUS GRAPHS

In this section, we first explore the label generation process in HGs from a causal perspective and introduce a novel structural causal model (SCM) to conceptualize this process. Next, we leverage this SCM to investigate the invariance principle in HGs. This principle serves as the foundation for enabling OOD generalization in HGFL.

A. Causal Perspective on Node Label Generation

Considering a target node v_t in an HG G, we construct an SCM to model the label generation process of v_t from a causal perspective (illustrated in Fig. 2). The rationale behind this SCM is explained as follows:

- E_1 represents observed original features of nodes and edges in G. We consider that E_1 is shaped by the underlying environmental context behind the HG. Different contexts can result in variations in the features of nodes and edges. For instance, in social networks, when user communities originating from various environments (e.g., users from different countries or having different professions) are modeled as HGs, they generally exhibit distinct user characteristics and interaction attributes.
- E_2 represents unobserved node and edge features in G. These features are typically elusive and not directly observable, such as the uniformity of user behaviors across different social networks and the general tendencies of consumers to follow purchasing trends in e-commerce networks. Unlike E_1 , E_2 is not affected by environmental changes (e.g., transitioning from students' social communities to celebrities' social communities), and there is no direct causal relationship between E_1 and E_2 . Therefore, we consider E_1 and E_2 to be independent of each other. Moreover, both E_1 and E_2 include node-level and edge-level features but lack compound semantic information, making them global yet shallow in nature.
- G_s denotes the observed subgraph structure comprising v_t and its neighbors. Specifically, G_s can be extracted using methods like considering the k-hop neighbors of v_t in G.
- Z_1 and Z_2 represent semantics associated with the target node v_t , which are local yet high-level in nature. Z_1 includes semantics influenced by E_1 and G_s , while Z_2 represents those only affected by E_2 .
- Y denotes the category or label assigned to v_t .
- $(E_1, E_2) \rightarrow G_s$ means that the subgraph structure is determined by features of nodes and edges around v_t .

- (E₁, G_s) → Z₁ and E₂ → Z₂ denote that high-level semantics are derived from the combinations of shallow-level node and edge features. Z₁ and Z₂ are unobservable and typically require domain-specific knowledge for identification. For instance, researchers often utilize predefined meta-paths [37] and meta-graphs [38] that consist of diverse node types to extract semantic information.
- $(Z_1, Z_2, G_s) \rightarrow Y$ means that the label of v_t is determined by high-level semantics and the subgraph structure.

Connection with Existing Works and Novel Insights. While our proposed SCM is the first causal model for node label generation in HGs, our analysis reveals that the SCM not only aligns with established paradigms in the existing literature but also introduces some novel insights:

- Capturing semantics in HGs from shallow level to high level: Since directly capturing complex semantics within HGs is challenging [39], existing methods typically adopt a hierarchical learning strategy, leveraging diverse node types to capture complex heterogeneous information and reveal underlying semantics [20], [21]. Differently, our SCM extends this approach by focusing on semantics in OOD environments. We adopt a causality-driven perspective to derive semantics from shallow-level features.
- Leveraging semantics for node labeling: Investigating node-related semantics is crucial for accurate node classification [40], [41]. Existing methods tend to focus on explicit semantic information within individual HGs. In contrast, our SCM highlights the importance of invariant implicit semantic information across various HGs, providing a new perspective on node labeling in OOD environments.
- Extracting semantics from subgraphs: Several studies have proved that local subgraphs can retain substantial node-related properties for node-level tasks [16], [42]. Our SCM extends this notion by delving into the causal connections between subgraphs and node features. we aim to identify unobservable, environment-independent node features during the subgraph generation process, thereby achieving a more comprehensive understanding of semantic extraction.

B. Exploring Invariance for OOD Generalization on HGs

In our proposed SCM, a distribution shift occurs when there are changes in at least one of the observed factors (i.e., E_1 , G_s and Y). In this work, we focus on the *covariate shift* [43], [44] scenario where the input features (E_1 and G_s) change while the conditional distribution of the label ($P(Y|G_s, E_1)$) stays the same. Specifically, we denote E_1 and G_s in one HG as e_1 and e_1 , respectively, and in another HG as e_1 and e_2 . From a causal view, the distribution shift from ($e_1 = e_1$, $e_2 = e_2$) to ($e_2 = e_1$) is formulated as an *intervention* [45], denoted as $e_1 = e_2$, $e_2 = e_2$. Therefore, OOD generalization in HGs can be modeled as a *post-intervention inference* of node label probabilities $e_1 = e_2$, $e_2 = e_2$.

Considering that the intervention $do(E_1 = \mathbf{e}_1', G_s = \mathbf{g}')$ only affects Z_1 , we can reuse the unaffected parts E_2 and Z_2 to perform post-intervention inference. Thus, the invariance principle for OOD generalization in HGs is that models are invariant to distribution shifts if they focus only on unaffected

variables E_2 and Z_2 . Since Z_2 is only determined by E_2 and can be inferred from it, identifying E_2 is the main challenge.

V. METHODOLOGY

A. Overview

In this section, we introduce our Causal OOD Heterogeneous graph Few-shot learning model, named COHF. COHF follows our SCM structure and utilizes unaffected variables $(E_2 \text{ and } Z_2)$ to mitigate distribution shifts in HGFL. (1) To achieve effective knowledge transfer, COHF proposes a variational autoencoder-based HGNN (VAE-HGNN). VAE-HGNN first models causal relations within the SCM and then applies causal inference on these relations to identify E_2 and Z_2 . By integrating this VAE-HGNN with a meta-learning framework, the knowledge of extracting unaffected variables can be transferred from the source HG to the target HG. (2) To facilitate stable class learning from few-labeled samples, COHF proposes a node valuator module that evaluates the importance of each sample. By prioritizing samples with rich invariant features, COHF can effectively capture class information that remains consistent despite distribution shifts.

B. Variational Autoencoder-based HGNN

Fig. 3 illustrates the architecture of VAE-HGNN, which is closely aligned with the structure of our proposed SCM. VAE-HGNN includes three main modules to model the three unobservable variables in the SCM, i.e., E_2 , Z_1 and Z_2 , respectively. (1) The relation encoder module infers the unobserved node features E_2 by leveraging the observed node features E_1 and the subgraph structure G_s . (2) The multi-layer GNN module infers the semantics Z_1 based on E_1 and G_s . (3) The graph learner module infers Z_2 based on the previously inferred E_2 . Overall, VAE-HGNN integrates an encoder that infers E_2 , and a decoder that employs E_1 , E_2 , and G_s to predict the label Y. Causal Inference for OOD Generalization in HGs. Before a distribution shift occurs, we represent all observed variables as $(E_1 = \mathbf{e_1}, G_s = \mathbf{g}, Y = \mathbf{y})$. Since the variable $E_2 = \mathbf{e_2}$ remains invariant to distribution shifts, our goal is to infer e2 conditional on these observed variables, i.e., to estimate the posterior distribution $p_{\theta}(\mathbf{e_2}|\mathbf{y},\mathbf{e_1},\mathbf{g})$, which is parameterized by θ . However, this distribution is intractable due to the complexity of the joint distribution $p(y, e_1, g)$. To address this challenge, we resort to variational inference [46], [47] and introduce a variational distribution $q_{\phi}(\mathbf{e_2}|\mathbf{y},\mathbf{e_1},\mathbf{g})$, parameterized by ϕ , to approximate the true posterior $p_{\theta}(\mathbf{e_2}|\mathbf{y},\mathbf{e_1},\mathbf{g})$. **Learning Objective.** Following the VAE mechanism in [47], [48], we optimize the model parameters θ and ϕ by maximizing the Evidence Lower BOund (ELBO), which is a lower bound for the log-likelihood of the observed data:

$$\log p_{\theta}(\mathbf{y}, \mathbf{g} | \mathbf{e_1}) \ge \mathbb{E}_{q_{\phi}(\mathbf{e_2} | \mathbf{y}, \mathbf{g}, \mathbf{e_1})} \left[\log p_{\theta}(\mathbf{y}, \mathbf{g} | \mathbf{e_1}, \mathbf{e_2}) \right] - KL \left[q_{\phi}(\mathbf{e_2} | \mathbf{y}, \mathbf{g}, \mathbf{e_1}) \| p(\mathbf{e_2}) \right]$$

$$\triangleq -\mathcal{L}_{ELBO},$$
(1)

the detailed proof can be found in Appendix I.

The rationale behind Eq. (1) is that minimizing the ELBO loss \mathcal{L}_{ELBO} corresponds to maximizing the log-likelihood of

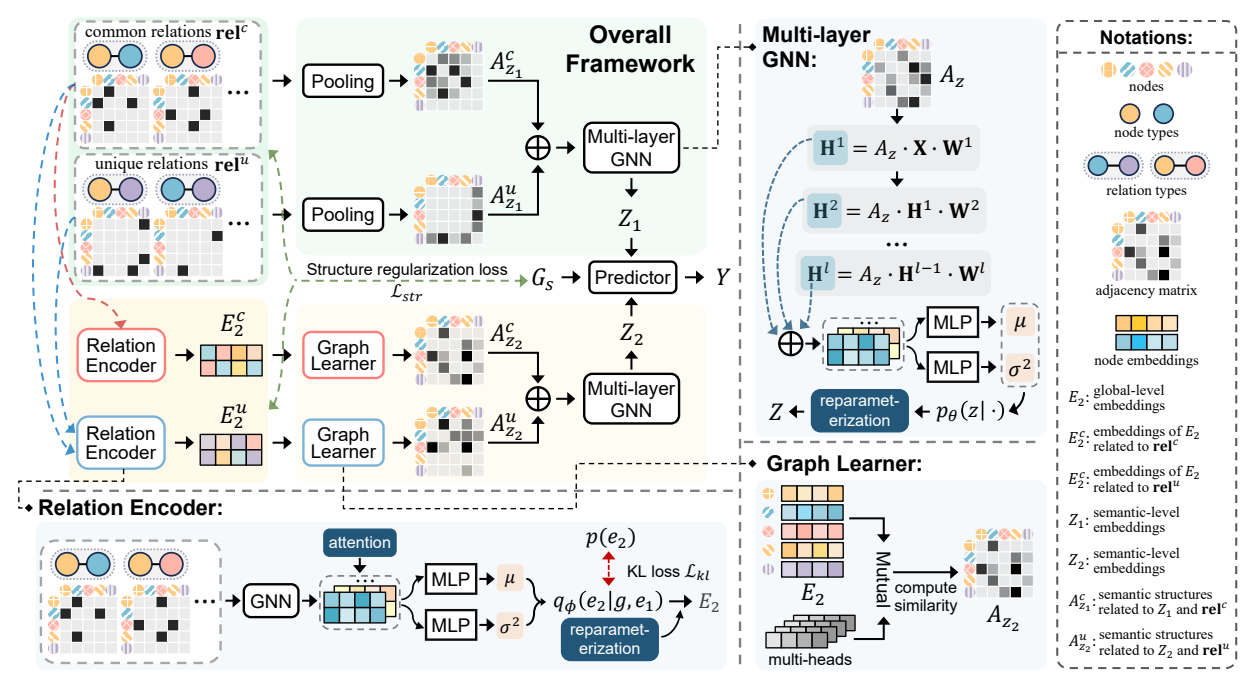


Fig. 3. The overall architecture of VAE-HGNN.

the observed data y and g conditioned on e_1 . The learning objective can be further elaborated as follows:

$$\mathcal{L}_{ELBO} = \underbrace{-\mathbb{E}_{q_{\phi}(\mathbf{e_2}|\mathbf{y},\mathbf{g},\mathbf{e_1})}[\log p_{\theta}(\mathbf{y}|\mathbf{g},\mathbf{e_1},\mathbf{e_2})]}_{\text{Classification Loss } \mathcal{L}_{cls}} \underbrace{-\mathbb{E}_{q_{\phi}(\mathbf{e_2}|\mathbf{y},\mathbf{g},\mathbf{e_1})}[\log p_{\theta}(\mathbf{g}|\mathbf{e_1},\mathbf{e_2})]}_{\text{Structure Regularization Loss } \mathcal{L}_{str}} + \underbrace{KL[q_{\phi}(\mathbf{e_2}|\mathbf{y},\mathbf{g},\mathbf{e_1})||p(\mathbf{e_2})]}_{\text{KL Loss } \mathcal{L}_{bl}},$$
(2)

where the first two terms account for the node label and subgraph structure regeneration, respectively, while the last term regularizes the Kullback-Leibler (KL) divergence between $q_{\phi}(\mathbf{e_2}|\mathbf{y},\mathbf{g},\mathbf{e_1})$ and $p(\mathbf{e_2})$. We assume that $\mathbf{e_2}$ is a D-dimensional latent vector sampled from a standard Gaussian prior [49], i.e., $p(\mathbf{e_2}) = \mathcal{N}(0,\mathbf{I}_D)$. To compute \mathcal{L}_{ELBO} , we design an encoder $f_{\phi}(\cdot)$ to model $q_{\phi}(\mathbf{e_2}|\mathbf{y},\mathbf{g},\mathbf{e_1})$; and two decoders $g_{\theta_1}(\cdot)$ and $g_{\theta_2}(\cdot)$ to model $p_{\theta}(\mathbf{y}|\mathbf{g},\mathbf{e_1},\mathbf{e_2})$ and $p_{\theta}(\mathbf{g}|\mathbf{e_1},\mathbf{e_2})$, respectively.

Encoder Network. To instantiate the posterior distribution q_{ϕ} , we first make a further approximation from $q_{\phi}(\mathbf{e_2}|\mathbf{y},\mathbf{g},\mathbf{e_1})$ to $q_{\phi}(\mathbf{e_2}|\mathbf{g},\mathbf{e_1})$. This approximation is known as the mean-field method, which is widely used in variational inference [50], [51]. Note that although \mathbf{y} is not directly used as input for the encoder, it serves as the supervision information for the training process. Inspired by variational autoencoders [47], we define $q_{\phi}(\mathbf{e_2}|\mathbf{g},\mathbf{e_1})$ as a multivariate Gaussian with a diagonal covariance structure, which is flexible and allows \mathcal{L}_{ELBO} to be computed analytically [49]. Accordingly, the encoder is designed as follows:

$$\mathbf{h}_{\mathbf{e_2}} = \text{GNN}_{\phi}(\mathbf{g}, \mathbf{e_1}), \tag{3}$$

$$q_{\phi}(\mathbf{e_2}|\mathbf{g}, \mathbf{e_1}) = \mathcal{N}\left(\mu_{\phi}(\mathbf{h_{e_2}}), \operatorname{diag}\{\sigma_{\phi}^2(\mathbf{h_{e_2}})\}\right),$$
 (4)

where $\mathrm{GNN}_{\phi}(\cdot)$ is a graph neural network that transforms subgraph structures and node features into latent representations $\mathbf{h}_{\mathbf{e_2}}.\ \mu_{\phi}(\cdot)$ and $\sigma_{\phi}(\cdot)$ are multi-layer perceptrons (MLPs) that convert $\mathbf{h}_{\mathbf{e_2}}$ into the mean and standard deviations, respectively, to parameterize the distribution of $q_{\phi}(\mathbf{e_2}|\mathbf{g},\mathbf{e_1})$. Since $q_{\phi}(\mathbf{e_2}|\mathbf{g},\mathbf{e_1})$ takes on a Gaussian form, the reparameterization trick from variational autoencoders [47] can be employed here to calculate derivatives w.r.t. the encoder parameters.

 $\mathrm{GNN}_\phi(\cdot)$ is designed to derive node representations that are related to E_2 , which are robust to distribution shifts in E_1 and G_s . Given that there are three levels of distribution shifts in OOD environments within HGFL: feature-level, topology-level, and heterogeneity-level, our design of $\mathrm{GNN}_\phi(\cdot)$ is guided by the following considerations:

- Considering feature-level shifts, *i.e.*, variations in node and edge features, since we focus on addressing the node classification problem, $\text{GNN}_{\phi}(\cdot)$ transforms \mathbf{g} and $\mathbf{e_1}$ into nodelevel hidden representations. These representations should be stable and unaffected by variations in node/edge features.
- Considering topology-level shifts, GNN_φ(·) should be able to capture heterogeneous information that is not affected by changes in the graph structure. However, existing GNNs typically capture heterogeneous information through specific graph patterns (e.g., meta-paths and meta-graphs [21], [38]), which may not persist after topology-level shifts. Therefore, we choose to focus more on the simple components of these graph patterns, i.e., node-node relations (such as paperauthor). Topology-level shifts may lead to changes in meta-paths and meta-graphs, but the information of these fundamental relations remains unaffected [52] and can be combined to capture higher-level semantics.
- Considering heterogeneity-level shifts between two HGs G_1 and G_2 , differences in node types between the two HGs can lead to different relation types. Therefore,we categorize

relation types from the two HGs into two sets: \mathbf{rel}^c that includes common relation types in both HGs, and \mathbf{rel}^u that contains unique relation types for each HG. Formally, $\mathbf{rel}^c = \{(\Phi_i, \Phi_j) | (\Phi_i, \Phi_j) \in \mathcal{S}_n^1, (\Phi_i, \Phi_j) \in \mathcal{S}_n^2\}$, where Φ_i and Φ_j are two node types in G_1 and G_2 , respectively, and \mathcal{S}_n^1 and \mathcal{S}_n^2 are the node type sets of G_1 and G_2 , respectively. $\mathbf{rel}_1^u = \{(\Phi_i, \Phi_j) | (\Phi_i, \Phi_j) \in \mathcal{S}_n^1, (\Phi_i, \Phi_j) \notin \mathcal{S}_n^2\}$ is the unique relation set in G_1 . Thus, a heterogeneity-level shift from $E_1 = \mathbf{e}_1$ to $E_1 = \mathbf{e}_1'$ implies that $\mathbf{rel}^c(\mathbf{e}_1) = \mathbf{rel}^c(\mathbf{e}_1')$ while $\mathbf{rel}^u(\mathbf{e}_1) \cup \mathbf{rel}^u(\mathbf{e}_1') \neq \emptyset$.

Based on the above analysis, we propose two subgraph-based relation encoders, $f_{\phi}^{c}(\cdot)$ and $f_{\phi}^{u}(\cdot)$, to learn the distributions of $\mathbf{e_2}$ related to \mathbf{rel}^c and \mathbf{rel}^u , denoted as $q_{\phi}(\mathbf{e_2^c}|\mathbf{g},\mathbf{e_1})$ and $q_{\phi}(\mathbf{e_2^u}|\mathbf{g},\mathbf{e_1})$, respectively. Specifically, we first extract n_k -hop neighbors of the target node v_t to construct the subgraph structure G_s . Then, we use the adjacency matrices of \mathbf{rel}^c and \mathbf{rel}^u in G_s , denoted as \mathbf{A}^c and \mathbf{A}^u respectively, as the input for $f_{\phi}^c(\cdot)$ and $f_{\phi}^u(\cdot)$. Formally, $\mathbf{A}^c = \{A_{i,j} | (\Phi_i, \Phi_j) \in \mathbf{rel}^c \}$ and $\mathbf{A}^u = \{A_{i,j} | (\Phi_i, \Phi_j) \in \mathbf{rel}^u \}$, where the adjacency matrix $A_{i,j} = \{a_{mn} | m, n \in \mathcal{V}_s, \varphi(m) = \Phi_i, \varphi(n) = \Phi_j \}$, here a_{mn} is the connectivity between nodes m and n.

For invariant feature extraction from \mathbf{rel}^c and \mathbf{rel}^u , we assume that both relations contain features that remain unaffected by distribution shifts. For \mathbf{rel}^c , the invariant features are inherent within the relations themselves. In contrast, for \mathbf{rel}^u , the invariant features arise from the interactions between \mathbf{rel}^c and \mathbf{rel}^u . These interactions essentially reflect the mechanism by which common relations interact with unique relations. Specifically, for the common relation encoder $f_\phi^c(\cdot)$, we first employ a GNN to learn the representation of a node v under the i-th relation type $r_i \in \mathbf{rel}^c$:

$$\mathbf{h}_{v-i}^{c} = \text{GNN}_{c} \left(A_{i}^{c}, \mathbf{x}_{v} \right), \tag{5}$$

where $A_i^c \in \mathbf{A}^c$ is the adjacency matrix of r_i , \mathbf{x}_v is the original feature of node v. Then, we adopt an attention mechanism to aggregate information from different relation types in \mathbf{rel}^c :

$$\alpha_{v-i}^{c} = \frac{\exp\left(\text{ReLU}\left(\mathbf{a}_{c}^{\mathsf{T}} \cdot \mathbf{h}_{v-i}^{c}\right)\right)}{\sum_{j=1}^{|\mathbf{rel}^{c}|} \exp\left(\text{ReLU}\left(\mathbf{a}_{c}^{\mathsf{T}} \cdot \mathbf{h}_{v-j}^{c}\right)\right)},$$
 (6)

$$\mathbf{h}_{v}^{c} = \sum_{i=1}^{|\mathbf{r}\mathbf{e}|^{c}} \alpha_{v-i}^{c} \cdot \mathbf{h}_{v-i}^{c}, \tag{7}$$

where $\alpha^c_{v\cdot i}$ denotes the importance of the *i*-th type in \mathbf{rel}^c , and \mathbf{a}_c represents the trainable attention parameter shared among all common relation types. The unique relation encoder $f^u_\phi(\cdot)$ has the same structure as $f^c_\phi(\cdot)$ but processes different inputs. Specifically, when learning the representations of nodes under a unique relation, we consider integrating the interaction between the unique relation and common relations \mathbf{A}^c into another GNN:

$$\mathbf{h}_{v-i}^{u} = \text{GNN}_{u} \left(A_{i}^{u} \cdot f_{pool}^{c} \left(\mathbf{A}^{c} \right), \mathbf{x}_{v} \right), \tag{8}$$

where A_i^u is the adjacency matrix of *i*-th unique relation, and $f_{pool}^c(\cdot)$ is a pooling function (e.g., $max-pool(\cdot)$, $sum-pool(\cdot)$, and $mean-pool(\cdot)$). Then, in the attention mechanism, we con-

catenate the representations of common relations and unique relations to compute the importance of each unique relation:

$$\alpha_{v-i}^{u} = \frac{\exp\left(\operatorname{ReLU}\left(\mathbf{a}_{u}^{\mathsf{T}} \cdot [\mathbf{h}_{v-i}^{u} \| \mathbf{h}_{v}^{c}]\right)\right)}{\sum_{j=1}^{|\mathbf{rel}^{u}|} \exp\left(\operatorname{ReLU}\left(\mathbf{a}_{u}^{\mathsf{T}} \cdot [\mathbf{h}_{v-j}^{u} \| \mathbf{h}_{v}^{c}]\right)\right)},\tag{9}$$

$$\mathbf{h}_{v}^{u} = \sum_{i=1}^{|\mathbf{rel}^{u}|} \alpha_{v-i}^{u} \cdot \mathbf{h}_{v-i}^{u}, \tag{10}$$

where $\alpha_{v cdot i}^u$ denotes the importance of the *i*-th type in \mathbf{rel}^u , and \mathbf{a}_u represents the trainable attention parameter shared among all unique relation types. Finally, following Eq. (19), we input \mathbf{h}^c and \mathbf{h}^u into different MLPs to compute the distributions of $q_\phi(\mathbf{e}_2^\mathbf{c}|\mathbf{g}, \mathbf{e}_1)$ and $q_\phi(\mathbf{e}_2^\mathbf{c}|\mathbf{g}, \mathbf{e}_1)$, respectively.

Decoder Networks. We propose two decoder networks $g_{\theta_1}(\cdot)$ and $g_{\theta_2}(\cdot)$ to model $p_{\theta}(\mathbf{y}|\mathbf{g}, \mathbf{e_1}, \mathbf{e_2})$ and $p_{\theta}(\mathbf{g}|\mathbf{e_1}, \mathbf{e_2})$, respectively. For $g_{\theta_1}(\cdot)$, we first factorize $p_{\theta}(\mathbf{y}|\mathbf{g}, \mathbf{e_1}, \mathbf{e_2})$ based on our proposed SCM as follows:

$$p_{\theta}(\mathbf{y}|\mathbf{g}, \mathbf{e_1}, \mathbf{e_2}) = \int_{\mathbf{z_1}} \int_{\mathbf{z_2}} p_{\theta}(\mathbf{z_1}|\mathbf{g}, \mathbf{e_1}) p_{\theta}(\mathbf{z_2}|\mathbf{e_2})$$

$$p_{\theta}(\mathbf{y}|\mathbf{g}, \mathbf{z_1}, \mathbf{z_2}) d\mathbf{z_1} d\mathbf{z_2}.$$
(11)

Based on the above factorization result, the core idea of $g_{\theta_1}(\cdot)$ is utilizing node features $E_1 = \mathbf{e_1}$ and $E_2 = \mathbf{e_2}$ to capture complex semantics $Z_1 = \mathbf{z_1}$ and $Z_2 = \mathbf{z_2}$, and then employing $\mathbf{z_1}$ and $\mathbf{z_2}$ with \mathbf{g} to predict the label \mathbf{y} . We consider that Z_1 and Z_2 are semantic-level features derived from specific graph structures determined by $\mathbf{e_1}$ and $\mathbf{e_2}$, respectively. Accordingly, we first evaluate the connectivity of nodes influenced by $\mathbf{e_1}$ and $\mathbf{e_2}$, generating distinct graph structures that represent different semantics. Then, we implement representation learning within these specific graph structures. Next, we will detail the instantiation of each factorized distribution.

Instantiating $p_{\theta}(\mathbf{z}_1|\mathbf{g}, \mathbf{e}_1)$ with Multi-layer GNN: We utilize various meta-paths in the subgraph $G_s = \mathbf{g}$ to capture semantics derived from $E_1 = \mathbf{e}_1$. A meta-path consists of diverse node types and conveys specific semantics [21]. For example, author-paper-author indicates author collaboration. Existing works typically require manually defined meta-paths [37]. However, in scenarios involving distribution shifts and few-shot learning, setting and sampling significant meta-paths is challenging [53]. Therefore, we propose a multi-layer GNN that automatically captures both short and long meta-paths across various relations. For adjacency matrices of common relations (\mathbf{A}^c) and unique relations (\mathbf{A}^u), each relation matrix can be considered as a 1-length meta-path graph matrix. We first combine \mathbf{A}^c and \mathbf{A}^u to construct a weighted 1-length meta-path graph matrix:

$$A_{z_1} = \beta_{z_1} \times f_{pool}^{z_1}(\mathbf{A}^c) + (1 - \beta_{z_1}) \times f_{pool}^{z_1}(\mathbf{A}^u), \tag{12}$$

where β_{z_1} is a trainable smoothing parameter. To extract longer meta-paths, successive multiplications can be performed on the matrix A_{z_1} . For example, raising A_{z_1} to the second power automatically incorporates information about 2-length metapaths. This approach is commonly employed in existing metapath extraction methods [22], [54]. Therefore, to capture more

diverse and longer meta-paths, we extend this approach to a network structure with l layers as follows:

$$\mathbf{H}_{z_{1}}^{(l)} = A_{z_{1}} \cdot \mathbf{H}_{z_{1}}^{(l-1)} \cdot \mathbf{W}_{z_{1}}^{(l)}$$

$$= \underbrace{A_{z_{1}} \cdots (A_{z_{1}}}_{l} \cdot \mathbf{X} \cdot \underbrace{\mathbf{W}_{z_{1}}^{(1)}) \cdots \mathbf{W}_{z_{1}}^{(l)}}_{l}$$

$$= A_{z_{1}}^{l} \cdot \mathbf{X} \cdot \underbrace{\mathbf{W}_{z_{1}}^{(1)} \cdots \mathbf{W}_{z_{1}}^{(l)}}_{l},$$

$$(13)$$

where $\mathbf{H}_{z_1}^{(l)}$ is the hidden embedding of the l-th layer, \mathbf{X} is the node feature matrix of G_s , and $\mathbf{W}_{z_1}^{(l)}$ is the learnable weight matrix that evaluates the influence of meta-paths with l-length on the embedding. Finally, we fuse the outputs of all layers to capture the meta-path information of different lengths across various relations as follows:

$$\mathbf{H}_{z_{1}} = \frac{1}{l} \sum_{i=1}^{l} \mathbf{H}_{z_{1}}^{(i)}$$

$$= \frac{1}{l} \sum_{i=1}^{l} A_{z_{1}}^{l} \cdot \mathbf{H}_{z_{1}}^{(i-1)} \cdot \mathbf{W}_{z_{1}}^{(i)},$$
(14)

where $\mathbf{H}_{z_1}^{(0)}$ is the node feature matrix \mathbf{X} . Then, we adopt two MLPs $\mu_{\theta_{z_1}}(\cdot)$ and $\sigma_{\theta_{z_1}}(\cdot)$ to estimate the parameters of $p_{\theta}(\mathbf{z_1}|\mathbf{g}, \mathbf{e_1})$ as follows:

$$p_{\theta}(\mathbf{z_1}|\mathbf{g}, \mathbf{e_1}) = \mathcal{N}\left(\mu_{\theta_{z_1}}(\mathbf{H}_{z_1}), \operatorname{diag}\{\sigma_{\theta_{z_1}}^2(\mathbf{H}_{z_1})\}\right). \tag{15}$$

Instantiating $p_{\theta}(\mathbf{z_2}|\mathbf{e_2})$ with Graph Learner: We first sample $\mathbf{e_2^c}$ and $\mathbf{e_2^u}$ from the distributions learned by the encoder networks, *i.e.*, $q_{\phi}(\mathbf{e_2^c}|\mathbf{y},\mathbf{g},\mathbf{e_1})$ and $q_{\phi}(\mathbf{e_2^u}|\mathbf{y},\mathbf{g},\mathbf{e_1})$, respectively. Since $\mathbf{z_2}$ does not depend on the subgraph structure \mathbf{g} , we reconstruct the node connectivity regarding common and unique relations based on the node features of $\mathbf{e_2^c}$ and $\mathbf{e_2^u}$. Then, we leverage a Multi-layer GNN to capture semantics based on the reconstructed graph structure. Specifically, we propose two graph learner modules to construct adjacency matrices for $\mathbf{e_2^c}$ and $\mathbf{e_2^u}$, denoted as $A_{z_2}^c$ and $A_{z_2}^u$, respectively. In each graph learner module, a multi-head weighted cosine similarity learning method is used to compute the connectivity of nodes as follows:

$$a_{uv}^c = \frac{1}{n_{att}} \sum_{i=1}^{n_{att}} \cos\left(\mathbf{w}_i^c \cdot \mathbf{h}_u^{e_2}, \mathbf{w}_i^c \cdot \mathbf{h}_v^{e_2}\right), \tag{16}$$

where $\mathbf{h}_{u}^{e_{2}}$ and $\mathbf{h}_{v}^{e_{2}}$ are node representations in $\mathbf{e}_{\mathbf{c}}^{\mathbf{c}}$ for a node pair (u,v), the set $\{\mathbf{w}_{i}^{c}\}_{i=1}^{n_{att}}$ consists of n_{att} independent learnable weight vectors, which perform similarly as attention mechanisms [55]. After obtaining $A_{z_{2}}^{c}$ and $A_{z_{2}}^{u}$, we adopt a trainable parameter $\beta_{z_{2}}$ to aggregate them and use Multi-layer GNN to learn the semantic-level representation of Z_{2} :

$$A_{z_2} = \beta_{z_2} \times A_{z_2}^c + (1 - \beta_{z_2}) \times A_{z_2}^u, \tag{17}$$

$$\mathbf{H}_{z_2} = \mathrm{GNN}_{z_2} \left(A_{z_2}, \mathbf{X} \right). \tag{18}$$

Finally, two MLPs $\mu_{\theta_{z_2}}(\cdot)$ and $\sigma_{\theta_{z_2}}(\cdot)$ are used to estimate the parameters of $p_{\theta}(\mathbf{z_2}|\mathbf{e_2})$:

$$p_{\theta}(\mathbf{z_2}|\mathbf{e_2}) = \mathcal{N}\left(\mu_{\theta_{z_2}}(\mathbf{H}_{z_2}), \operatorname{diag}\{\sigma_{\theta_{z_2}}^2(\mathbf{H}_{z_2})\}\right). \tag{19}$$

Approximating $p_{\theta}(\mathbf{y}|\mathbf{g}, \mathbf{z_1}, \mathbf{z_2})$: Even if we obtain the estimations of $p_{\theta}(\mathbf{z_1}|\mathbf{g}, \mathbf{e_1})$ and $p_{\theta}(\mathbf{z_2}|\mathbf{e_2})$, the calculation of $p_{\theta}(\mathbf{y}|\mathbf{g}, \mathbf{z_1}, \mathbf{z_2})$ remains challenging due to the costly integral over the latent variables $\mathbf{z_1}$ and $\mathbf{z_2}$. To achieve higher efficiency, we resort to Monte Carlo (MC) sampling, which samples $\mathbf{z_1}$ and $\mathbf{z_2}$ to approximate $p_{\theta}(\mathbf{y}|\mathbf{g}, \mathbf{z_1}, \mathbf{z_2})$:

$$p_{\theta}(\mathbf{y}|\mathbf{g}, \mathbf{z_1}, \mathbf{z_2}) \approx \frac{1}{L} \frac{1}{M} \sum_{i=1}^{L} \sum_{j=1}^{M} p_{\theta} \left(\mathbf{y}|\mathbf{g}, \mathbf{z}_1^i, \mathbf{z}_2^j \right),$$
 (20)

where L and M are the sample numbers; \mathbf{z}_1^i and \mathbf{z}_2^j are drawn from $p_{\theta}(\mathbf{z_1}|\mathbf{g}, \mathbf{e_1})$ and $p_{\theta}(\mathbf{z_2}|\mathbf{e_2})$, respectively. Nevertheless, Eq. (20) is still computationally costly due to calculating the conditional probability many times (*i.e.*, $L \times M$). We thus further conduct a widely used approximation [56], [57], which is formulated as follows:

$$p_{\theta}(\mathbf{y}|\mathbf{g}, \mathbf{z_1}, \mathbf{z_2}) \approx p_{\theta} \left(\mathbf{y} \left| \mathbf{g}, \frac{1}{L} \sum_{i=1}^{L} \mathbf{z}_1^i, \frac{1}{M} \sum_{j=1}^{M} \mathbf{z}_2^j \right) \right.$$

$$= p_{\theta}(\mathbf{y}|\mathbf{g}, \overline{\mathbf{z}_1}, \overline{\mathbf{z}_2}). \tag{21}$$

The approximation error (i.e., Jensen gap [58]) can be well bounded for most functions to calculate $p_{\theta}(\mathbf{y}|\mathbf{g}, \overline{\mathbf{z}_1}, \overline{\mathbf{z}_2})$ [56]. Thereafter, we use a GNN to incorporate \mathbf{g} with $\overline{\mathbf{z}_1}$ and $\overline{\mathbf{z}_2}$ into final embeddings:

$$\mathbf{h} = \text{GNN}_{y} \left(A_{g}, [\bar{\mathbf{z}}_{1} || \bar{\mathbf{z}}_{2}] \right). \tag{22}$$

where A_g is the adjacency matrix of G_s . Finally, we model $p_{\theta}(\mathbf{y}|\mathbf{g}, \mathbf{z_1}, \mathbf{z_2})$ with an MLP that utilizes \mathbf{h} to produce a probability distribution over multiple classes.

Instantiating $p_{\theta}(\mathbf{g}|\mathbf{e_1}, \mathbf{e_2})$ with Latent Space Model: We specify $p_{\theta}(\mathbf{g}|\mathbf{e_1}, \mathbf{e_2})$ by modelling the distribution of edges in \mathbf{g} under the condition of $\mathbf{e_1}$ and $\mathbf{e_2}$. Let $a_{ij} \in \mathcal{V} \times \mathcal{V}$ represent the binary edge random variable between node i and node j. $a_{ij} = 1$ indicates the edge between i and j exists and 0 otherwise. A general assumption used by various generative models for graphs is that the edges are conditionally independent [59]. Therefore, $p_{\theta}(\mathbf{g}|\mathbf{e_1}, \mathbf{e_2})$ can be factorized as follows:

$$p_{\theta}(\mathbf{g}|\mathbf{e_1}, \mathbf{e_2}) = \prod_{i,j} p_{\theta} \left(a_{ij} | \mathbf{e_1}, \mathbf{e_2} \right). \tag{23}$$

Next, we adopt the latent space model (LSM) [60], which is a widely used generative network model in the network science literature. LSM assumes that the nodes lie in a latent space and the probability of a_{ij} only depends on the representations of nodes i and j, i.e., $p_{\theta_2}(a_{ij}|\mathbf{e_1},\mathbf{e_2}) = p_{\theta_2}(a_{ij}|\mathbf{e_1},\mathbf{e_1}^j,\mathbf{e_2}^i,\mathbf{e_2}^j)$. We assume it follows a logistic regression model:

$$p_{\theta}(a_{ij} = 1 | \mathbf{e}_{\mathbf{1}}^{i}, \mathbf{e}_{\mathbf{1}}^{j}, \mathbf{e}_{\mathbf{2}}^{i}, \mathbf{e}_{\mathbf{2}}^{j})$$

$$= \delta \left(\boldsymbol{w}^{\mathsf{T}} \left[\mathbf{U}(\mathbf{x}_{i}), \mathbf{U}(\mathbf{x}_{j}), \left[\mathbf{e}_{\mathbf{2}}^{c-i} || \mathbf{e}_{\mathbf{2}}^{u-i} \right], \left[\mathbf{e}_{\mathbf{2}}^{c-j} || \mathbf{e}_{\mathbf{2}}^{u-j} \right] \right] \right),$$
(24)

where $\delta(\cdot)$ is the sigmoid function; \boldsymbol{w} are the learnable parameters of the logistic regression model; $\mathbf{U}(\cdot)$ is a linear transformation function. $\mathbf{e}_{\mathbf{2}}^{c\cdot i}$ and $\mathbf{e}_{\mathbf{2}}^{u\cdot i}$ denote the embeddings of node i sampled from $q_{\phi}(\mathbf{e}_{\mathbf{2}}^{\mathbf{c}}|\mathbf{y},\mathbf{g},\mathbf{e}_{\mathbf{1}})$ and $q_{\phi}(\mathbf{e}_{\mathbf{2}}^{\mathbf{u}}|\mathbf{y},\mathbf{g},\mathbf{e}_{\mathbf{1}})$, respectively. We concatenate the transformed features and node embeddings as the input of the logistic regression model. All learnable parameters are included in θ .

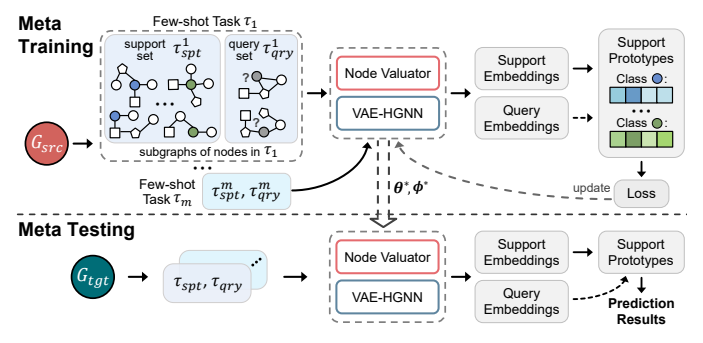


Fig. 4. Meta-learning Framework.

C. Meta-Learning

Fig. 4 illustrates an overview of our proposed meta-learning framework, which consists of two steps: meta-training and meta-testing. In meta-training, we utilize few-shot tasks on the source HG to train VAE-HGNN, where a novel *node valuator* module is proposed to determine the informativeness of each labeled node. Then, we adopt a prototypical network to transfer generalized knowledge from the source HG to the target HG. During meta-testing, the node valuator is adapted to the target HG to evaluate the importance of few-labeled nodes in OOD environments, thereby facilitating the generation of robust class representations for prediction.

Node Valuator. Evaluating the importance of few-labeled samples is a prevalent strategy in existing graph few-shot learning methods [4], [61]. The general evaluation approach prioritizes nodes with notable centrality and popularity. However, this approach may not be appropriate for OOD environments, where the source HG and target HG might have distinct node degree distributions.

To address this issue, we adopt a causal perspective to evaluate the importance of labeled nodes in OOD environments. We focus on evaluating the richness of node features that remain robust against distribution shifts and determine whether these features are distinctly identifiable. Based on our proposed SCM, we consider the following two aspects: (1) Since Z_2 is unaffected by distribution shifts and directly influences the label Y, we investigate node features associated with Z_2 . (2) As Z_1 is influenced by changes in E_1 and G_s , to effectively learn the features of Z_2 without interference from the features of Z_1 , node features related to Z_2 should be distinguishable from those related to Z_1 . Specifically, we evaluate the node importance from its structural-level and node-level features:

- 1. Structure-level features: Since the semantic features of Z_1 and Z_2 are extracted from specific graph structures, having distinctive features related to Z_2 implies that the structural differences between Z_2 and Z_1 should be maximized. Furthermore, the graph structure behind Z_2 should exhibit a certain degree of connectivity, as insufficient connectivity may result in a structure that lacks meaningful semantics.
- **2. Node-level features:** The node features in Z_1 and Z_2 should also be distinctly different. However, directly comparing the representations of the same node in Z_1 and Z_2 can be influenced by Z_1 and Z_2 the node's inherent characteristics, which are present in both Z_1 and Z_2 . Therefore, we propose

incorporating the features of neighboring nodes as a reference for more effective comparison.

For the richness of structure-level features, we compare the similarity between $A_{z_1}^{sum}$ and A_{z_2} , and assess the connectivity of A_{z_2} . Here, $A_{z_1}^{sum} = \frac{1}{l} \sum_{i=1}^{l} A_{z_1}^{l}$ is derived from the Multi-layer GNN module as described in Eq. (14), while A_{z_2} is obtained from the graph learner module as outlined in Eq. (17). The richness score of the structure-level features is defined as:

$$\operatorname{rsl}(v_t) = \cos\left(A_{z_1}^{sum}, A_{z_2}\right) + \log\left(\frac{\sum_{i=1}^{|\mathcal{V}_s|} \deg_{z_2}(v_i)}{|\mathcal{V}_s|} + \epsilon\right), (25)$$

where ϵ is a small constant, $\deg_{z_2}(v_i)$ is the in-degree of node v_i in A_{z_2} , and $|\mathcal{V}_s|$ is the number of nodes in the subgraph of v_t (i.e., G_s). For node-level features, we first compute the richness score for each neighbor v_n of v_t :

$$\operatorname{sn}(v_t, v_n) = \operatorname{tanh}\left(\mathbf{W}_s \cdot \left[\mathbf{h}_{v_t}^{z_1} \| \mathbf{h}_{v_n}^{z_2} \right]\right), \tag{26}$$

where $\mathbf{h}_{v_n}^{z_2}$ represents the embedding of v_n sampled from $p_{\theta}(\mathbf{z_2}|\mathbf{e_2})$, and $\mathbf{h}_{v_t}^{z_1}$ represents the embedding of v_t sampled from $p_{\theta}(\mathbf{z_1}|\mathbf{g},\mathbf{e_1})$. \mathbf{W}_s is a learnable weight matrix. Then, we adopt an attention mechanism to compute the importance of the neighbor v_n and compute the node-level richness score:

$$\gamma_{tn} = \frac{\exp\left(\text{LeakyReLU}\left(\mathbf{a}_{s}^{\mathsf{T}}\left[\mathbf{h}_{v_{t}}^{z_{2}} \| \mathbf{h}_{v_{n}}^{z_{2}}\right]\right)\right)}{\sum_{v_{j} \in \mathbf{Nei}_{t}} \exp\left(\text{LeakyReLU}\left(\mathbf{a}_{s}^{\mathsf{T}}\left[\mathbf{h}_{v_{j}}^{z_{2}} \| \mathbf{h}_{v_{n}}^{z_{2}}\right]\right)\right)}, \quad (27)$$

$$\operatorname{rnl}(v_t) = \sum_{v_i \in \mathbf{Nei}_t} \gamma_{ti} \cdot \operatorname{sn}(v_t, v_i), \tag{28}$$

where \mathbf{Nei}_t is the set of neighbors of v_t in A_{z_2} , and \mathbf{a}_s is the trainable attention parameter. Finally, the richness score of a labeled node can be computed as $rs(v_t) = rsl(v_t) + rrnl(v_t)$.

Prototypical Network. We follow the idea of the prototypical network [62] and calculate the weighted average of K-shot embedded nodes within class c to derive the class prototype:

$$\mathbf{proto}_c = \sum_{i=1}^K \mathbf{sc}_i \cdot \mathbf{h}_{v_i}, \tag{29}$$

where $sc_i = rs(v_i) / \sum_{j=1}^K rs(v_j)$ is the normalized score, h_{v_i} is the final embedding of node v_i output by VAE-HGNN. The node valuator module is trained through meta-training and is used to compute the class prototype in meta-testing.

Loss Function. During meta-training, the prototype for each class is computed using the nodes in the support set τ^{spt} . To determine the class of a query node u in the query set τ^{qry} , we calculate the probability for each class based on the distance between the node embedding \mathbf{h}_u and each prototype:

$$\operatorname{prob}(c|u) = \frac{\exp\left(-\operatorname{d}(\mathbf{h}_u, \mathbf{proto}_c)\right)}{\sum_{c'} \exp\left(-\operatorname{d}(\mathbf{h}_u, \mathbf{proto}_{c'})\right)},$$
 (30)

where $d(\cdot)$ is a distance metric function and we adopt squared Euclidean distance [62]. Under the episodic training framework, the objective of each meta-training task is to minimize the classification loss between the predictions of the query set and the ground truth. The training loss for a single task τ is the average negative log-likelihood probability of assigning correct class labels as follows:

$$\mathcal{L}_{\tau} = -\frac{1}{N \times K} \sum_{i=1}^{N \times K} \log \left(\operatorname{prob}(y_i^* | v_i) \right), \qquad (31)$$

where y_i^* is the ground truth label of v_i . Then, by incorporating VAE-HGNN with the ELBO loss ($\mathcal{L}_{ELBO} = \mathcal{L}_{cls} + \mathcal{L}_{str} + \mathcal{L}_{kl}$). prob $(y_i^*|v_i)$ can be modeled by $p_{\theta}(\mathbf{y}|\mathbf{g}, \mathbf{e_1}, \mathbf{e_2})$ and thus $\mathcal{L}_{\tau} = \mathcal{L}_{cls}$. Finally, the total meta-training loss can be defined as:

$$\mathcal{L}_{meta} = \sum_{j=1}^{|\mathcal{T}_{src}|} \mathcal{L}_{cls}^{j} + \mathcal{L}_{str}^{j} + \lambda \cdot \mathcal{L}_{kl}^{j}, \tag{32}$$

where λ is a loss coefficient hyper-parameter to restrict the regularization of the KL divergence.

D. Efficiency Analysis

Targeting the novel and complex OOD generalization in HG few-shot learning, our proposed COHF is efficient due to the following properties:

Subgraph-based Few-shot Learning: COHF extracts subgraphs surrounding labeled nodes for learning, rather than processing the entire graph structure. By integrating causal learning, COHF further focuses on structures that have a causal relationship with the labels. This approach ensures that the input graph size and the learning graph structure remain small and consistent during computation, leading to stable memory consumption and improved computational efficiency.

Concise, Hierarchical Semantic Information Extraction: Unlike traditional heterogeneous GNNs that rely on multiple modules to capture diverse heterogeneous information for learning semantics, COHF focuses on extracting heterogeneous information only from common and unique relations. Additionally, COHF leverages a structure causal model to identify invariant semantics from shallow level to high level. This approach simplifies the few-shot learning framework in OOD environments and ensures that COHF's computational complexity remains unaffected by the complexity of the heterogeneous information.

Furthermore, we conduct experiments to compare the time and memory consumption of COHF and the baselines in the same OOD scenarios. See Appendix III for comparison results.

VI. EXPERIMENTS AND ANALYSIS

We conduct extensive experiments on seven real-world datasets to answer the following research questions: **RQ1**: How does COHF perform compared with representative and state-of-the-art methods in OOD environments? **RQ2**: How does each of the proposed VAE-HGNN module and node valuator module contribute to the overall performance? **RQ3**: How does COHF perform under different parameter settings?

A. Experimental Settings

Datasets. We adopt seven real-world datasets from three domains: (1) ACM [22] and DBLP [21] from the academic research domain. (2) IMDB [21], MovieLens [63], and Douban [39] from the movie domain. (3) YELP-Restaurant (abbreviated as YELP-R) [52] and YELP-Business (abbreviated as YELP-B) [64] from the business domain. These datasets are publicly available and have been widely used in studies of HGs [39]. Details of these datasets are provided in Table II. **Meta-learning and OOD Settings.** We consider the following two distinct scenarios:

TABLE II STATISTICS OF DATASETS.

Domain	Dataset	# Nodes	# Relations
	ACM	# A-P: 9,936 # P-S: 3,025	
Academic	DBLP	# authors (A): 4,057 # papers (P): 14,328 # terms (T): 7,723 # venues (V): 20	# A-P: 19,645 # P-T: 85,810 # P-V: 14,328
	IMDB	# movies (M): 4,278 # directors (D): 2,081 # actors (A): 5,257	# M-D: 4,278 # M-A: 12,828
Movie	MovieLens	# movies (M): 1,682 # users (U): 943 # occupations (O): 21 # ages (E): 8	# U-M: 100,000 # U-E: 943 # U-O: 943
	Douban	# movies (M): 12,677 # directors (D): 2,449 # actors (A): 6,311 # users (U): 13,367 # groups (G): 2,753	# M-D: 11,276 # M-A: 33,587 # U-M: 355,072 # U-G: 127,632 # U-U: 392,519
Business	YELP-R	# businesses (B): 2,614 # users (U): 1,286 # services (S): 2 # star levels (L): 9 # reservations (R): 2	# B-U: 30,838 # B-R: 2,614 # B-S: 2,614 # B-L: 2,614
	YELP-B	# businesses (B): 7,474 # phrases (P): 74,943 # star levels (L): 9 # locations (O): 39	# B-P: 27,209,836 # B-L: 7,474 # B-O: 7,474 # P-P: 2,654,313

- 1. Inter-dataset setting: In this setting, two different datasets from the same domain are randomly selected as the source HG and the target HG. Note that there are inherent differences between datasets within the same domain, including variations in node and relationship types, different node features, and diverse graph structures. These differences result in multiple distribution shifts between the source HG and the target HG. Furthermore, to simulate distribution shifts between training and testing data in the target HG, we follow the approach in [44] to generate training and testing data with covariate shifts based on node degrees.
- 2. Intra-dataset setting: In this setting, both the source HG and the target HGs are derived from the same dataset. In few-shot learning, these two HGs must encompass distinct node classes (labels) for meta-training and meta-testing, respectively. This requirement mandates the selection of datasets with a substantial diversity of node classes. Consequently, we choose three out of the seven datasets containing more than ten node classes: Douban (38 movie node classes), MovieLens (18 movie node classes), and YELP-B (16 business node classes). For each dataset, the classes are divided into two groups to serve as labels the source HG and the target HG, respectively. Moreover, to evaluate the performance of methods in both the I.I.D. environment and the OOD environment, we generate I.I.D. and OOD data for each dataset:
- For I.I.D. data, we randomly divide the dataset into three splits with similar sizes, which are designated as the source HG, training data, and testing data.
- For OOD data, we firstly follow [44] to generate three splits with covariate shifts based on node degrees. Then, we introduce heterogeneity-level shifts by randomly reducing node types (excluding the target node type) in each of these three splits. These modified splits are then designated as the source HG, training data, and testing data.

 $\label{thm:local_transform} \textbf{TABLE III} \\ \textbf{NODE CLASSIFICATION ACCURACY IN INTER-DATASET SETTING.} \\$

Carl		ACM-	DBLP	DBLP	-ACM	IMDB-	Douban	Doubar	1-IMDB	MvLens	-Douban	Douban	-MvLens	YELI	YELP R-B		P B-R
GAT		2-way	3-way	2-way	3-way	2-way	3-way	2-way	3-way	2-way	3-way	2-way	3-way	2-way	3-way	2-way	3-way
SGC O.7147 O.6057 O.5698 O.4652 O.4932 O.3253 O.5147 O.33512 O.4953 O.3269 O.5174 O.3414 O.5077 O.3469 O.5118 O.3656 O.4508								1	-shot								
Cali	GAT	0.7133	0.5489	0.6297	0.4733	0.4017	0.3052	0.5167	0.3458	0.4590		0.5050	0.3458	0.5043	0.3413	0.5470	0.3544
HAN		1								1				l			
Macionn Color Co										<u> </u>				!			
UDAGCN										1							
Musdace		1								1							
CAL 0.5023 0.3288 0.5490 0.3296 0.4898 0.3219 0.5094 0.3370 0.4950 0.3367 0.4913 0.3352 0.5063 0.3339 0.5060 0.3412 DIR 0.5939 0.4880 0.6359 0.4943 0.4313 0.2710 0.5117 0.3477 0.4283 0.2632 0.4871 0.3229 0.5027 0.3345 0.5722 0.4284 WSGNN 0.5300 0.3489 0.5037 0.3347 0.3345 0.5030 0.3321 0.5030 0.3321 0.5030 0.3321 0.5030 0.3321 0.5030 0.3321 0.5030 0.3321 0.5030 0.3321 0.5030 0.3321 0.5030 0.3331 0.5030 0.3334 0.4767 0.3345 0.4767 0.3345 0.4758 0.3939 0.4838 0.319 0.5068 0.3436 0.4758 0.3332 0.5008 0.3384 0.4976 0.3317 0.5190 0.3338 0.5060 0.3334 0.5068 0.4758 0.4758 0.3458 0.5157 0.3473 0.4990 0.3338 0.5020 0.3334 0.5268 0.4968 0.4588 0.4948 0.4926 0.3335 0.5010 0.3334 0.5268 0.494														ı			
DIR N. 1939										l				<u> </u>			
MSGNN 0.5300 0.3489 0.5037 0.3347 0.5003 0.3321 0.4828 0.3240 0.5017 0.3345 0.4767 0.3408 0.5117 0.3186 0.4834 0.3267														l			
MAML ProtoNet		1												l			
ProtoNet 0.5580 0.3949 0.5636 0.3939 0.4838 0.3119 0.5068 0.3436 0.4758 0.2986 0.5157 0.3473 0.4990 0.3338 0.5026 0.3439 Meta-GNN 0.7099 0.5915 0.6509 0.5312 0.4844 0.3261 0.5167 0.3448 0.4924 0.3334 0.5227 0.3523 0.5002 0.3324 0.5336 GPN 0.6122 0.4518 0.7099 0.5355 0.4501 0.2920 0.5032 0.3289 0.3898 0.5004 0.3337 0.5049 0.3333 0.5010 0.3334 0.5127 0.4016 GPN 0.66879 0.5377 0.5744 0.4007 0.4907 0.4048 0.5370 0.3273 0.4795 0.3301 0.5194 0.3929 0.5145 0.3665 0.5291 0.3768 CGFL 0.8240* 0.7211* 0.7413 0.6049 0.5158* 0.3080 0.5374* 0.3714* 0.5290* 0.3153 0.5467 0.3701 0.5358* 0.3769* 0.6509* 0.4797* HG-Meta 0.7940 0.7031 0.7337 0.5631 0.5038 0.3167 0.5320 0.3653 0.4610 0.2944 0.5514* 0.3840 0.5216 0.3489 0.6316 0.4699 Improvement* 2.148* 2.278* 4.038* 3.818* 3.228* 6.088* 5.698* 6.198* 5.568* 1.3698* 7.299* 3.519* 6.555* 6.858* 3.279* 2.068* GAT 0.8162 0.6733 0.6760 0.5549 0.4067 0.3122 0.5429 0.3880 0.4416 0.2622 0.5355 0.4014 0.5189 0.3469 0.5509 0.4987 GIN 0.7694 0.6204 0.6787 0.5542 0.3990 0.2975 0.5487 0.3888 0.4764 0.2428 0.5429 0.4376 0.5093 0.3619 0.6662 0.5118 HAN 0.8795 0.7532 0.8233 0.6052 0.4923 0.3491 0.5583 0.3962* 0.3770 0.2824 0.5631 0.3932 0.5267 0.3667 0.6811 0.5378 MAGNN 0.8912 0.7641 0.8328* 0.5220 0.5075* 0.3445 0.5120 0.3445 0.5543 0.3932 0.5500 0.3440 0.5189 0.5157 0.3457 0.3459 0.5066 0.3490 0.5157 0.3457 0.3538 0.3661 0.3938 0.5060 0.3409 0.5004 0.3341 0.55130 0.3469 0.5066 0.3391 0.5666 0.3391 0.5666 0.3391 0.5662 0.5181 0.5664 0.5157 0.3458 0.5665 0.3458 0.5665 0.3459 0.5665 0.3459 0.5665 0.3459 0.4662 0.5189 0.4662 0.5189 0.4662										1							
GPN G-Meta 0.6122 0.4518 0.7099 0.5355 0.4501 0.2920 0.5032 0.3389 0.5004 0.3337 0.4928 0.3335 0.5010 0.3334 0.5127 0.4016 CGFL HG-Meta 0.8249° 0.7211* 0.7413 0.6049 0.5150° 0.3808 0.5374* 0.3714* 0.3290* 0.3135 0.5467 0.3701 0.5358* 0.3665 0.5291* 0.3708 COHF Improvement* 0.8416* 0.7375 0.7530 0.6407 0.5316 0.3611 0.5680 0.3944 0.5584 0.3944 0.5514* 0.3940 0.5106 0.4067 0.5709 0.4067 Improvement* 2.148 2.278 4.038 3.818* 3.228* 6.088* 5.698* 6.199* 5.566* 1.3698* 7.298* 3.516* 6.559* 0.4067 Improvement* 2.148* 0.6733 0.6760 0.5549 0.4087 0.5120 0.3489 0.5290 0.3812 0.5622 0.3880 0.4416 <t< td=""><td></td><td>I</td><td></td><td></td><td></td><td></td><td></td><td></td><td></td><td>1</td><td></td><td></td><td></td><td></td><td></td><td></td><td></td></t<>		I								1							
GPN G-Meta 0.6122 0.4518 0.7099 0.5355 0.4501 0.2920 0.5032 0.3389 0.5004 0.3337 0.4928 0.3335 0.5010 0.3334 0.5127 0.4016 CGFL HG-Meta 0.8249° 0.7211* 0.7413 0.6049 0.5150° 0.3808 0.5374* 0.3714* 0.3290* 0.3135 0.5467 0.3701 0.5358* 0.3665 0.5291* 0.3708 COHF Improvement* 0.8416* 0.7375 0.7530 0.6407 0.5316 0.3611 0.5680 0.3944 0.5584 0.3944 0.5514* 0.3940 0.5106 0.4067 0.5709 0.4067 Improvement* 2.148 2.278 4.038 3.818* 3.228* 6.088* 5.698* 6.199* 5.566* 1.3698* 7.298* 3.516* 6.559* 0.4067 Improvement* 2.148* 0.6733 0.6760 0.5549 0.4087 0.5120 0.3489 0.5290 0.3812 0.5622 0.3880 0.4416 <t< td=""><td>Meta-GNN</td><td>0.7099</td><td>0.5915</td><td>0.6509</td><td>0.5312</td><td>0.4844</td><td>0.3261</td><td>0.5167</td><td>0.3448</td><td>0.4924</td><td>0.3342</td><td>0.5227</td><td>0.3523</td><td>0.5002</td><td>0.3324</td><td>0.5316</td><td>0.3536</td></t<>	Meta-GNN	0.7099	0.5915	0.6509	0.5312	0.4844	0.3261	0.5167	0.3448	0.4924	0.3342	0.5227	0.3523	0.5002	0.3324	0.5316	0.3536
CGFL O.8240* 0.7211* 0.7413		1												ı			
HG-Meta 0.7940 0.7031 0.7337 0.5631 0.5038 0.3176 0.5320 0.3653 0.4610 0.2944 0.5514 0.3840 0.5216 0.3489 0.6316 0.4609	G-Meta	0.6879	0.5377	0.5744	0.4007	0.4907	0.3404*	0.5370	0.3273	0.4795	0.3301	0.5194	0.3929*	0.5145	0.3665	0.5291	0.3768
COHF	CGFL	0.8240*	0.7211*	0.7413	0.6049	0.5150*	0.3080	0.5374*	0.3714*	0.5290*	0.3153	0.5467	0.3701	0.5358*	0.3769*	0.6509*	0.4797*
Improvement 2.14% 2.27% 4.03% 3.81% 3.22% 6.08% 5.69% 6.19% 5.56% 13.69% 7.29% 3.51% 6.55% 6.85% 3.27% 2.06%	HG-Meta	0.7940	0.7031	0.7337	0.5631	0.5038	0.3176	0.5320	0.3653	0.4610	0.2944	0.5514*	0.3840	0.5216	0.3489	0.6316	0.4609
GAT 0.8162 0.6733 0.6760 0.5549 0.4067 0.3122 0.5429 0.3880 0.4416 0.2622 0.5355 0.4014 0.5189 0.3469 0.5509 0.4087 SGC 0.8107 0.6788 0.6944 0.5577 0.4878 0.3104 0.5461 0.3707 0.4790 0.3235 0.5065 0.4050 0.5031 0.3478 0.5416 0.4378 GIN 0.7694 0.6204 0.6787 0.5542 0.3909 0.2975 0.5457 0.3885 0.4764 0.2428 0.5429 0.4376 0.5093 0.3619 0.6662 0.5118 HAN 0.8795 0.7532 0.8233 0.6052 0.4923 0.3091 0.5583 0.3962* 0.3770 0.2824 0.5631 0.3932 0.5267 0.3667 0.6811 0.5378 MAGNN 0.8912 0.7641 0.8325* 0.5227 0.5075* 0.3445 0.5461 0.3937 0.5204 0.3441 0.5849 0.4522* 0.5255 0.3533 0.6930 0.4636 UDAGCN 0.5153 0.3498 0.5520 0.3480 0.5047 0.3442 0.5120 0.3453 0.5004 0.3222 0.5001 0.3331 0.5004 0.3341 0.5573 0.3661 CAL 0.5193 0.3382 0.4974 0.3303 0.4917 0.3229 0.5183 0.3352 0.5053 0.3393 0.5307 0.3370 0.5106 0.3313 0.5130 0.3457 DIR 0.6897 0.5600 0.6760 0.5371 0.4333 0.2880 0.5339 0.3658 0.4343 0.2932 0.5060 0.3400 0.5157 0.3547 0.6323 0.4704 WSGNN 0.4518 0.3378 0.5133 0.3412 0.5011 0.3444 0.5122 0.3341 0.3346 0.3370 0.5011 0.3526 0.4822 0.4987 0.3037 0.5104 0.3369 0.4988 0.3307 0.5106 0.3341 0.5052 0.3572 ProtoNet 0.5634 0.4175 0.5438 0.4968 0.4962 0.3345 0.5048 0.3347 0.5014 0.3369 0.4986 0.3409 0.5098 0.3413 0.5052 0.3574 Meta-GNN 0.8328 0.6939 0.7429 0.6126 0.4953 0.3341 0.5443 0.3708 0.4998 0.3415 0.4703 0.3071 0.512 0.3576 0.5710 0.4569 G-Meta 0.7324 0.5114 0.6958 0.6027 0.4965 0.3569* 0.4919 0.411 0.5056 0.3433 0.5056 0.3478 0.5247 0.3912* 0.6833 0.3222 CGFL 0.9241* 0.8178* 0.8207 0.6368 0.4956 0.3444 0.5643* 0.3896 0.5598 0.3571 0.4569 0.5988 0.4424 0.5254 0.3575 0.5858 0.		0.84161	0.7375	0.7753	0.6407	0.5316	0.3611	0.5680		0.5584	0.3944	0.5916	0.4067	0.5709	0.4027	0.6722	0.4896
GAT 0.8162 0.6733 0.6760 0.5549 0.4067 0.3122 0.5429 0.3880 0.4416 0.2622 0.5355 0.4014 0.5189 0.3469 0.5509 0.4087 SGC 0.8107 0.6788 0.6944 0.5577 0.4878 0.3104 0.5461 0.3707 0.4790 0.3235 0.5065 0.4050 0.5031 0.3478 0.5416 0.4378 GIN 0.7694 0.6204 0.6787 0.5542 0.3909 0.2975 0.5457 0.3888 0.4764 0.2428 0.5429 0.4376 0.5093 0.3619 0.6662 0.5118 0.8707 0.8912 0.7641 0.8325* 0.5227 0.5075* 0.3445 0.5461 0.3937 0.5204 0.3441 0.5849 0.4522* 0.5255 0.3533 0.6930 0.4636 0.4923 0.4923 0.5018 0.5120 0.3453 0.5004 0.3242 0.5011 0.3331 0.5004 0.3341 0.5322 0.3517 0.3422 0.5224 0.5631 0.3932 0.5555 0.3533 0.6930 0.4636 0.4923 0.5018 0.5180 0.3413 0.5180 0.3413 0.5322 0.5018 0.3414 0.5849 0.4522* 0.5255 0.3533 0.6930 0.4636 0.4924 0.5425 0.5255 0.3533 0.6930 0.4636 0.5424 0.5444 0.5424 0.5434 0.4915	Improvement ²	2.14%	2.27%	4.03%	3.81%	3.22%	6.08%	5.69%	6.19%	5.56%	13.69%	7.29%	3.51%	6.55%	6.85%	3.27%	2.06%
SGC 0.8107 0.6788 0.6944 0.5577 0.4878 0.3104 0.5461 0.3707 0.4790 0.3235 0.5065 0.4050 0.5031 0.3478 0.5416 0.4378 GIN 0.7694 0.6204 0.6787 0.5542 0.3909 0.2975 0.5457 0.3858 0.4764 0.2428 0.5429 0.4376 0.5093 0.3619 0.6662 0.5118 HAN 0.8795 0.7532 0.8233 0.6052 0.4923 0.3041 0.5583 0.3962* 0.3770 0.2824 0.5631 0.3932 0.5267 0.3667 0.6811 0.5378 MAGNN 0.8912 0.7641 0.8325* 0.5227 0.5075* 0.3442 0.5104 0.3441 0.5849 0.4522* 0.5255 0.3533 0.6930 0.4918 MuSDAC 0.5224 0.3646 0.5455 0.3882 0.5067 0.3431 0.5147 0.3422 0.5053 0.3333 0.5180 0.3413 0.5573 0.3661								3	3-shot								
GIN 0.7694 0.6204 0.6787 0.5542 0.3909 0.2975 0.5457 0.3858 0.4764 0.2428 0.5429 0.4376 0.5093 0.3619 0.6662 0.5118 HAN 0.8795 0.7532 0.8233 0.6052 0.4923 0.3091 0.5583 0.3962* 0.3770 0.2824 0.5631 0.3932 0.5267 0.3667 0.6811 0.5378 MAGNN 0.8912 0.7641 0.8325* 0.5227 0.5075* 0.3445 0.5461 0.3937 0.5204 0.3441 0.5849 0.4522* 0.5255 0.3533 0.6930 0.4636 UDAGCN 0.5153 0.3498 0.5520 0.3480 0.5047 0.3442 0.5120 0.3453 0.5004 0.3222 0.5001 0.3331 0.5104 0.3341 0.5520 0.3431 0.5147 0.3422 0.4987 0.3539 0.5180 0.3370 0.5180 0.3413 0.5520 0.3431 0.5520 0.3431 0.5539 0.3658 0										1							
HAN 0.8795 0.7532 0.8233 0.6052 0.4923 0.3091 0.5583 0.3962* 0.3770 0.2824 0.5631 0.3932 0.5267 0.3667 0.6811 0.5378 MAGNN 0.8912 0.7641 0.8325* 0.5227 0.5075* 0.3445 0.5461 0.3937 0.5204 0.3441 0.5849 0.4522* 0.5255 0.3533 0.6930 0.4636 UDAGCN 0.5153 0.3498 0.5520 0.3480 0.5047 0.3442 0.5120 0.3453 0.5044 0.3222 0.5001 0.3331 0.5004 0.3341 0.5322 0.3517 MuSDAC 0.5193 0.3382 0.4974 0.3303 0.4917 0.3229 0.5183 0.3352 0.5053 0.3393 0.5307 0.3313 0.5180 0.3413 0.5130 0.3342 0.5053 0.3393 0.5307 0.3510 0.3313 0.5130 0.3457 DIR 0.6897 0.5600 0.6760 0.5371 0.4333 0.2880																	
MAGNN 0.8912 0.7641 0.8325* 0.5227 0.5075* 0.3445 0.5461 0.3937 0.5204 0.3441 0.5849 0.4522* 0.5255 0.3533 0.6930 0.4636 UDAGCN 0.5153 0.3498 0.5520 0.3480 0.5047 0.3442 0.5120 0.3453 0.5004 0.3222 0.5011 0.3331 0.5004 0.3341 0.5322 0.3517 MuSDAC 0.5224 0.3664 0.5455 0.3882 0.5067 0.3431 0.5147 0.3422 0.4887 0.3258 0.5147 0.3489 0.5180 0.3413 0.5573 0.3661 CAL 0.5193 0.3382 0.4974 0.3303 0.4917 0.3229 0.5183 0.3352 0.5053 0.3393 0.5307 0.3510 0.3413 0.5130 0.3444 0.5182 0.3433 0.2486 0.4946 0.4841 0.5122 0.3341 0.25053 0.3393 0.5307 0.3400 0.5156 0.3313 0.5130 0.3434 <t< td=""><td></td><td></td><td></td><td></td><td></td><td></td><td></td><td></td><td></td><td></td><td></td><td></td><td></td><td>l</td><td></td><td></td><td></td></t<>														l			
UDAGCN 0.5153 0.3498 0.5520 0.3480 0.5047 0.3442 0.5120 0.3453 0.5004 0.3222 0.5001 0.3331 0.5004 0.3341 0.5322 0.3517 MuSDAC 0.5224 0.3664 0.5455 0.3882 0.5067 0.3431 0.5147 0.3422 0.4987 0.3258 0.5147 0.3489 0.5180 0.3413 0.5573 0.3661 CAL 0.5193 0.3382 0.4974 0.3303 0.4917 0.3229 0.5183 0.3352 0.5053 0.3393 0.5307 0.3370 0.5106 0.3313 0.5130 0.3457 DIR 0.6897 0.5600 0.6760 0.5371 0.4333 0.2880 0.5339 0.3658 0.4343 0.2932 0.5060 0.3400 0.5157 0.3547 0.6323 0.4704 WSGNN 0.4518 0.3378 0.5183 0.3444 0.5122 0.3341 0.3586 0.3370 0.5011 0.3482 0.3489 0.4878 0.3378 <td></td>																	
MuSDAC 0.5224 0.3664 0.5455 0.3882 0.5067 0.3431 0.5147 0.3422 0.4987 0.3258 0.5147 0.3489 0.5180 0.3413 0.5573 0.3661 CAL 0.5193 0.3382 0.4974 0.3303 0.4917 0.3229 0.5183 0.3352 0.5053 0.3393 0.5307 0.3370 0.5106 0.3313 0.5130 0.3457 DIR 0.6897 0.5600 0.6760 0.5371 0.4333 0.2880 0.5339 0.3658 0.4343 0.2932 0.5060 0.3400 0.5157 0.3547 0.6323 0.4704 WSGNN 0.4518 0.3378 0.5183 0.3412 0.5011 0.3444 0.5122 0.3341 0.3586 0.3370 0.5011 0.3452 0.4878 0.3479 MAML 0.7288 0.5409 0.6248 0.4962 0.3325 0.5084 0.3347 0.5014 0.3369 0.4986 0.3409 0.5098 0.3413 0.5052 0.3572		1								1				<u> </u>			
CAL 0.5193 0.3382 0.4974 0.3303 0.4917 0.3229 0.5183 0.3352 0.5053 0.3393 0.5307 0.3370 0.5106 0.3313 0.5130 0.3457 DIR 0.6897 0.5600 0.6760 0.5371 0.4333 0.2880 0.5339 0.3658 0.4343 0.2932 0.5060 0.3400 0.5157 0.3547 0.6323 0.4704 WSGNN 0.4518 0.3378 0.5183 0.3412 0.5011 0.3444 0.5122 0.3341 0.3586 0.3370 0.5011 0.3422 0.3489 0.4878 0.3378 MAML 0.7288 0.5409 0.6248 0.4962 0.3345 0.5084 0.3347 0.5014 0.3369 0.4986 0.3409 0.5098 0.3413 0.5052 0.3572 ProtoNet 0.5634 0.4175 0.5438 0.4285 0.4992 0.3325 0.5036 0.3397 0.4988 0.3307 0.5174 0.3495 0.5066 0.3332 0.5062 <td></td>																	
DIR WSGNN 0.6897 0.4518 0.5600 0.378 0.6760 0.5371 0.4333 0.3412 0.2880 0.5011 0.3339 0.3444 0.3658 0.3347 0.4343 0.3586 0.2932 0.3370 0.5060 0.5011 0.3400 0.5526 0.4822 0.3489 0.4878 0.3489 0.4704 0.4878 MAML ProtoNet 0.7288 0.5634 0.5409 0.4175 0.4968 0.4285 0.4962 0.4992 0.3345 0.3325 0.5084 0.5036 0.3347 0.5084 0.3369 0.4988 0.3307 0.4986 0.3409 0.3409 0.3409 0.5098 0.3409 0.5098 0.3413 0.5052 0.3552 0.3572 0.3544 Meta-GNN 0.7631 0.5636 0.6726 0.4903 0.4942 0.4962 0.3311 0.5442 0.5043 0.3311 0.5498 0.3015 0.3498 0.3411 0.3435 0.3498 0.3409 0.3409 0.3409 0.3499 0.3495 0.3495 0.3498 0.3497 0.3411 0.4988 0.3437 0.3411 0.4986 0.3433 0.3415 0.4915 0.3415 0.4916 0.3497 0.3415 0.4916 0.3411 0.5416 0.4998 0.3411 0.4916 0.3411 0.5412 0.3411 0.4916 0.3411 0.5412 0.3411 0.4916 0.3411 0.5412 0.3411 0.4916 0.34111 0.5412 0.3411 0.4916 0.3411 0.4916 0.3411 0.4916 0.3411 0.4916 0.34111 0.4916 0.3411 0.										1				l			
WSGNN 0.4518 0.3378 0.5183 0.3412 0.5011 0.3444 0.5122 0.3341 0.3586 0.3370 0.5011 0.3526 0.4822 0.3489 0.4878 0.3378 MAML ProtoNet 0.7288 0.5409 0.6248 0.4962 0.3345 0.5084 0.3347 0.5014 0.3369 0.4986 0.3409 0.5098 0.3413 0.5052 0.3572 ProtoNet 0.5634 0.4175 0.5438 0.4285 0.4992 0.3325 0.5036 0.3397 0.4988 0.3307 0.5174 0.3495 0.5066 0.3392 0.5062 0.3544 Meta-GNN 0.8328 0.6939 0.7429 0.6126 0.4953 0.3341 0.5443 0.3708 0.4998 0.3435 0.5502 0.3759 0.4995 0.3334 0.5498 0.3625 GPN 0.7631 0.5636 0.6726 0.4903 0.3452 0.311 0.3461 0.44915 0.3415 0.4703 0.3071 0.512 0.3576 <																	
MAMIL 0.7288 0.5409 0.6248 0.4968 0.4962 0.3345 0.5084 0.3347 0.5014 0.3369 0.4986 0.3409 0.5098 0.3413 0.5052 0.3572 ProtoNet 0.5634 0.4175 0.5438 0.4285 0.4992 0.3325 0.5036 0.3397 0.4988 0.3307 0.5174 0.3495 0.5066 0.3392 0.5062 0.3544 Meta-GNN 0.8328 0.6939 0.7429 0.6126 0.4953 0.3341 0.5443 0.3708 0.4998 0.3435 0.5502 0.3759 0.4995 0.3334 0.5498 0.3625 GPN 0.7631 0.5636 0.6726 0.4903 0.4542 0.3015 0.5154 0.3461 0.4915 0.3415 0.4703 0.3071 0.512 0.3576 0.5710 0.4569 G-Meta 0.7324 0.5114 0.6958 0.6027 0.4965 0.3444 0.5643* 0.3896 0.3333 0.6056* 0.3778 0.5247 0.																	
ProtoNet 0.5634 0.4175 0.5438 0.4285 0.4992 0.3325 0.5036 0.3397 0.4988 0.3307 0.5174 0.3495 0.5066 0.3392 0.5062 0.3544 Meta-GNN 0.8328 0.6939 0.7429 0.6126 0.4953 0.3341 0.5443 0.3708 0.4998 0.3435 0.5502 0.3759 0.4995 0.3344 0.5498 0.3625 GPN 0.7631 0.5636 0.6726 0.4903 0.4542 0.3015 0.5154 0.3461 0.4915 0.3415 0.4703 0.3071 0.512 0.3576 0.5710 0.4569 G-Meta 0.7324 0.5114 0.6958 0.6027 0.4965 0.3569* 0.4919 0.3411 0.5056 0.3433 0.6056* 0.3778 0.5247 0.3912* 0.6833 0.3222 CGFL 0.9241* 0.8178* 0.8207 0.6368 0.4956 0.3444 0.5643* 0.3896 0.3571 0.5823 0.4116 0.5404* <t< td=""><td></td><td>l</td><td></td><td></td><td></td><td></td><td></td><td></td><td></td><td>l</td><td></td><td></td><td></td><td><u> </u></td><td></td><td></td><td></td></t<>		l								l				<u> </u>			
Meta-GNN 0.8328 0.6939 0.7429 0.6126 0.4953 0.3341 0.5443 0.3708 0.4998 0.3435 0.5502 0.3759 0.4995 0.3334 0.5498 0.3625 GPN 0.7631 0.5636 0.6726 0.4903 0.4542 0.3015 0.5154 0.3461 0.4915 0.3415 0.4703 0.3071 0.512 0.3576 0.5710 0.4569 G-Meta 0.7324 0.5114 0.6958 0.6027 0.4965 0.3569* 0.4919 0.3411 0.5056 0.3433 0.6056* 0.3778 0.5247 0.3912* 0.6833 0.3222 CGFL 0.9241* 0.8178* 0.8207 0.6368 0.4956 0.3444 0.5643* 0.3896 0.3398* 0.3571 0.5823 0.4116 0.5404* 0.3815 0.6947* 0.5429* HG-Meta 0.9062 0.8136 0.7822 0.6478 0.5512 0.3889 0.6083 0.4319 0.5722 0.4056 0.6408 0.4612																	
GPN 0.7631 0.5636 0.6726 0.4903 0.4542 0.3015 0.5154 0.3461 0.4915 0.3415 0.4703 0.3071 0.512 0.3576 0.5710 0.4569 G-Meta 0.7324 0.5114 0.6958 0.6027 0.4965 0.3569* 0.4919 0.3411 0.5056 0.3433 0.6056* 0.3778 0.5247 0.3912* 0.6833 0.3222 CGFL 0.99241* 0.8178* 0.8207 0.6368 0.4956 0.3444 0.5643* 0.3896 0.3571 0.5823 0.4116 0.5404* 0.3815 0.6947* 0.5429* HG-Meta 0.9062 0.8136 0.7882 0.6491* 0.4672 0.2985 0.5564 0.3911 0.4766 0.3628* 0.5988 0.4424 0.5254 0.3575 0.5858 0.4224 COHF 0.9316 0.8263 0.8722 0.6778 0.5512 0.3889 0.6083 0.4319 0.5722 0.4056 0.6408 0.4612 0.5966 <t< td=""><td></td><td></td><td></td><td></td><td></td><td></td><td></td><td></td><td></td><td>1</td><td></td><td></td><td></td><td>·</td><td></td><td></td><td></td></t<>										1				·			
G-Meta 0.7324 0.5114 0.6958 0.6027 0.4965 0.3569* 0.4919 0.3411 0.5056 0.3433 0.6056* 0.3778 0.5247 0.3912* 0.6833 0.3222 CGFL 0.9241* 0.8178* 0.8207 0.6368 0.4956 0.3444 0.5643* 0.3896 0.5398* 0.3571 0.5823 0.4116 0.5404* 0.3815 0.6947* 0.5429* 0.9062 0.8136 0.7882 0.6491* 0.4672 0.2985 0.5564 0.3911 0.4766 0.3628* 0.5988 0.4424 0.5254 0.3575 0.5858 0.4224 COHF 0.9316 0.8263 0.8722 0.6778 0.5512 0.3889 0.6083 0.4319 0.5722 0.4056 0.6408 0.4612 0.5966 0.4194 0.7307 0.5611																	
HG-Meta 0.9062 0.8136 0.7882 0.6491* 0.4672 0.2985 0.5564 0.3911 0.4766 0.3628* 0.5988 0.4424 0.5254 0.3575 0.5858 0.4224 COHF 0.9316 0.8263 0.8722 0.6778 0.5512 0.3889 0.6083 0.4319 0.5722 0.4056 0.6408 0.4612 0.5966 0.4194 0.7307 0.5611		1								ı				l			
HG-Meta 0.9062 0.8136 0.7882 0.6491* 0.4672 0.2985 0.5564 0.3911 0.4766 0.3628* 0.5988 0.4424 0.5254 0.3575 0.5858 0.4224 COHF 0.9316 0.8263 0.8722 0.6778 0.5512 0.3889 0.6083 0.4319 0.5722 0.4056 0.6408 0.4612 0.5966 0.4194 0.7307 0.5611	CGFL	0.9241*	0.8178*	0.8207	0.6368	0.4956	0.3444	0.5643*	0.3896	0.5398*	0.3571	0.5823	0.4116	0.5404*	0.3815	0.6947*	0.5429*
		0.9062	0.8136	0.7882	0.6491*	0.4672	0.2985	0.5564		0.4766		0.5988	0.4424	0.5254	0.3575		
$Improvement^2 \mid \underline{0.81\%} \underline{1.04\%} \underline{4.77\%} \underline{4.42\%} \underline{8.61\%} \underline{8.97\%} \underline{7.80\%} \underline{9.01\%} \underline{6.00\%} \underline{11.80\%} \underline{5.81\%} \underline{1.99\%} \underline{10.40\%} \underline{7.21\%} \underline{5.18\%} \underline{3.35\%}$		0.9316	0.8263	0.8722	0.6778	0.5512	0.3889	0.6083	0.4319	0.5722	0.4056	0.6408	0.4612	0.5966	0.4194	0.7307	0.5611
	Improvement ²	0.81%	1.04%	<u>4.77%</u>	4.42%	8.61%	8.97%	7.80%	9.01%	6.00%	11.80%	5.81%	1.99%	10.40%	7.21%	5.18%	3.35%

^{*} Result of the best-performing baseline. 1 Results of the best-performing method are in bold. 2 Improvements of COHF over the best-performing baseline are underlined.

TABLE IV
NODE CLASSIFICATION F1-SCORE IN 2-WAY 3-SHOT SETTING.

	GAT	SGC	GIN	HAN	MAGNN	UDAGCN	MuSDAC	CAL	DIR	WSGNN	MAML	ProtoNet	Meta-GNN	GPN	G-Meta	CGFL	HG-Meta	COHF	Improv. ²
ACM-DBLP	0.8114	0.7973	0.7639	0.8648	0.8896	0.4889	0.5022	0.5193	0.6419	0.4540	0.6822	0.4736	0.8241	0.7520	0.6926	0.9136*	0.9041	$ 0.9289^1 $	1.67%
Douban-MvLens	0.5046	0.5056	0.5188	0.5486	0.5588	0.4532	0.5040	0.5285	0.4269	0.4710	0.4714	0.4452	0.5389	0.4208	0.6004*	0.5802	0.5807	0.6366	6.03%
YELP B-R	0.5269	0.5478	0.6172	0.6809	0.6879	0.5114	0.5367	0.4883	0.6127	0.4856	0.4887	0.4476	0.5456	0.5485	0.6812	0.6973*	0.5692	0.7251	3.99%
MvLens (I.I.D.)	0.5939	0.6012	0.6083	0.6501*	0.6345	0.5122	0.5113	0.5110	0.5362	0.5132	0.5090	0.4324	0.6105	0.5949	0.6447	0.6479	0.6426	0.6822	4.94%
MvLens (OOD)	0.5468	0.5134	0.5467	0.5813	0.5881	0.4932	0.4927	0.4973	0.4495	0.4697	0.4899	0.4138	0.5559	0.5353	0.6055	0.6183*	0.5887	0.6645	7.47%
Drop	7.93%	14.60%	10.13%	10.58%	7.31%	3.71%	3.64%	2.68%	16.17%	8.48%	3.75%	4.30%	8.94%	10.02%	6.08%	4.57%	8.39%	2.59%	

^{*} Result of the best-performing baseline. 1 Results of the best-performing method are in bold. 2 Improvements of COHF over the best-performing baseline are underlined.

We repeat the above two generation processes five times for each dataset, creating five I.I.D. and five OOD datasets. For one dataset under I.I.D. or OOD settings, we average the experimental results from its five corresponding generated datasets to derive the final results.

Baselines. Given the lack of specialized solutions for OOD generalization in HGFL problems, we select 17 representative and state-of-the-art methods as baselines, which can be adapted to our meta-learning and OOD settings with minor modifications. These baselines can be categorized into seven groups: 1) **Homogeneous GNNs:** *GAT* [65], *SGC* [66] and

GIN [67]; 2) Heterogeneous GNNs: HAN [20] and MAGNN [21]; 3) Unsupervised domain adaptive node classifications: UDA-GCN [34] and MuSDAC [35]; 4) Graph OOD generalization methods: CAL [31], DIR [13], and WSGNN [51]; 5) Few-shot learning methods: MAML [15] and ProtoNet [62]; 6) Homogeneous graph few-shot learning methods: Meta-GNN [23], GPN [61] and G-Meta [16]; 7) Heterogeneous graph few-shot learning methods: CGFL [4] and HG-Meta [7]. Details of these baselines are discussed in Appendix II.

Parameter Settings. In the *N*-way *K*-shot setting, *N* is set to $\{2, 3\}$ and *K* is set to $\{1, 3, 5\}$. The number of tasks *m* is set to

TABLE V Node classification accuracy in intra-dataset setting.

		Douban		N	IovieLer	ıs	YELP-B				
	I.I.D.	OOD	Drop	I.I.D.	OOD	Drop	I.I.D.	OOD	Drop		
			2	-way 1-s	hot						
GAT	0.5107	0.4560	10.71%	0.5477	0.5137	6.21%	0.5107	0.4933	3.41%		
SGC	0.5093	0.4983	2.16%	0.5563	0.5183	6.83%	0.5280	0.5152	2.42%		
GIN	0.5153	0.4813	6.60%	0.5743	0.5387	6.20%	0.5283	0.5094	3.58%		
HAN	0.5473	0.5233*	4.39%	0.5833	0.5567	4.56%	0.5517	0.5217	5.44%		
MAGNN	0.5522	0.5156	6.63%	0.6022	0.5633	6.46%	0.5544	0.5133	7.41%		
UDAGCN	0.5100	0.5042	1.14%	0.5033	0.5001	0.64%	0.5140	0.5101	0.76%		
MuSDAC	0.5153	0.5087	1.28%	0.5087	0.5060	0.53%	0.5267	0.5213	1.03%		
CAL	0.5018	0.4947	1.41%	0.5173	0.5019	2.98%	0.5127	0.5110	0.33%		
DIR	0.5142	0.4996	2.84%	0.5228	0.4893	6.41%	0.5117	0.5107	0.20%		
WSGNN	0.5042	0.4872	3.37%	0.5156	0.4978	3.45%	0.5211	0.5178	0.63%		
MAML	0.5063	0.5053	0.20%	0.5317	0.5157	3.01%	0.5223	0.5033	3.64%		
ProtoNet	0.5087	0.4893	3.81%	0.5427	0.5200	4.18%	0.5173	0.5003	3.29%		
Meta-GNN	0.5114	0.4773	6.67%	0.5473	0.5192	5.13%	0.5260	0.4964	5.63%		
GPN	0.5037	0.4717	6.35%	0.5550	0.5173	6.79%	0.5377	0.5037	6.32%		
G-Meta	0.5556	0.4889	12.01%		0.5326	6.18%	0.5859*	0.5222	10.87%		
CGFL	0.5612*	0.5077	9.53%	0.6289*	0.6011*	4.42%	0.5783	0.5433*	6.05%		
HG-Meta	0.5183	0.4817	7.06%	0.5933	0.5573	6.07%	0.5413	0.5207	3.81%		
COHF	0.58891	0.5681	3.53%	0.6392	0.6271	1.89%	0.6014	0.5853	2.68%		
Improvement ²	4.94%	8.56%		1.64%	4.33%		2.65%	7.73%			
				-way 3-s							
GAT	0.3436		22.32%		0.4018	15.91%	0.3556	0.3369	5.26%		
SGC	0.3447	0.2987	13.34%	0.4716		22.48%	0.3633	0.3309	8.92%		
GIN	0.3423	0.3049	10.93%			15.30%		0.3327	7.81%		
HAN	0.3612	0.3011	16.64%	0.4922	0.4456	9.47%	0.3744	0.3467	7.40%		
MAGNN	0.3581	0.3163	11.67%			11.15%	0.3756	0.3474	7.51%		
UDAGCN	0.3412	0.3309	3.02%	0.3356	0.3333	0.69%	0.3392	0.3351	1.21%		
MuSDAC	0.3471	0.3404	1.93%	0.3396	0.3356	1.18%	0.3404	0.3387	0.50%		
CAL	0.3413	0.3361	1.52%	0.3598	0.3442	4.34%	0.3469	0.3367	2.94%		
DIR	0.3467	0.3335 0.3404	3.81%	0.4044	0.3362	16.86%	0.3520	0.3404	3.30% 2.56%		
WSGNN	0.3433		0.84%	0.3615	0.3319	8.19%	0.3444	0.3356			
MAML ProtoNet	0.3424 0.3351	0.3309 0.3333	3.36% 0.54%	0.3464	0.3338 0.3484	3.64% 23.66%	0.3418 0.3384	0.3364 0.3331	1.58% 1.57%		
	l										
Meta-GNN GPN	0.3465	0.3274 0.3333	5.51% 4.11%	0.4961	0.4123 0.3873	16.89% 12.24%	0.3692 0.3722	0.3407 0.3322	7.72% 10.75%		
G-Meta	0.3476	0.3333	6.41%	0.4413	0.3873	18.85%	0.3764	0.3603	4.28%		
CGFL	0.3711*		5.44%	0.5259	0.4478		l .	0.3625*	4.56%		
HG-Meta	0.3652	0.3309**	6.57%	0.5239	0.4478	13.25%	0.3798**	0.3523**	4.36%		
COHF	0.3842	0.3412	1.74%	0.5313	0.4009	5.04%	0.3713	0.3331	0.66%		
Improvement ²		7.58%	1.74%	1.96%	9.01%	3.04%	3.08%	7.28%	0.00%		
mprovement	3.33/0	1.36/0		1.70 /0	<u>7.01 /0</u>		3.00 /6	1.20/0			

- * Result of the best-performing baseline
- Results of the best-performing method are in bold.
- ² Improvements of COHF over the best-performing baseline are underlined.

100 for all datasets. To ensure fair comparisons, the embedding dimension is set to 64 for both the baselines and COHF. The baseline parameters are initially set to the values reported in the original papers and are further optimized through grid-searching to achieve optimal performance. For COHF, the subgraph G_s is constructed by sampling 2-hop neighbors of the target node. The dimension of e_2 (D) is set to 64. In the relation encoder module, we adopt two GCNs [68] as GNN_c and GNN_u , $f_{pool}^c(\cdot)$ is set to $max-pooling(\cdot)$. In the multi-layer GNN module, $f_{pool}^{z_1}(\cdot)$ uses $max-pooling(\cdot)$, and the number of GNN layers (l) is set to 2. In the graph learner module, n_{att} is set to 8. We adopt GraphSAGE [69] as GNN_y . In the metalearning module, the loss coefficient λ is set to 0.4.

Evaluation Metrics. We adopt two widely used node classification metrics: *Accuracy* and *Macro-F1 score* [23], [65]. To ensure a fair and accurate assessment of the performance of all methods, we perform 10 independent runs for each *N*-way *K*-shot setting and report the average results.

B. Experimental Results

Performance Comparison with Baselines (RQ1). Tables III-V present the performance comparison between COHF and baselines in both inter-dataset and intra-dataset settings.

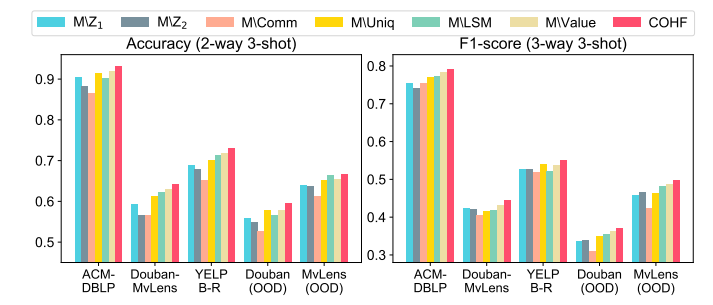


Fig. 5. Node classification performance of COHF variants.

The results demonstrate a significant improvement of COHF over the best-performing baselines. Across all settings, COHF consistently outperforms the baselines in terms of accuracy and F1-score. Specifically, in the inter-dataset setting, COHF achieves an average improvement of 5.66% in accuracy and 4.32% in F1-score. In the intra-dataset setting, COHF achieves an average increase of 5.19% in accuracy and 7.75% in F1score. These improvements are primarily attributed to our proposed VAE-HGNN module and the node valuator module. The VAE-HGNN module, innovatively designed based on our SCM model, effectively extracts invariant factors in OOD environments. Meanwhile, the node valuator module enhances knowledge transfer across HGs with distribution shifts and few-labeled data. In contrast, the baseline methods either overlook OOD environments in few-shot learning or focus solely on OOD problems within homogeneous graphs. Such limitations hinder their ability to extract generalized semantic knowledge from the source HG, leading to inferior performance when applied to a target HG with different distributions and limited labeled data.

Furthermore, it is worth noting that in Tables IV and V, almost all baseline methods demonstrate a significant drop in performance when transitioning from I.I.D. to OOD settings. This decline is especially evident in methods such as CGFL, G-Meta, and MAGNN, which perform well in I.I.D. settings. On average, there is a notable decrease of 6.28% in accuracy and 7.72% in F1-score across all baselines. In contrast, COHF exhibits a relatively minor average decrease of 2.8% in accuracy and 2.16% in F1-score. This underlines the robustness of our approach in handling distribution shifts in HGFL.

Ablation Study (RQ2). To investigate the impact of the core modules in COHF, we create six variants focusing on three key aspects: (1) Two variants are created to explore the effectiveness of the semantic features learned based on our proposed structural causal model. The $M \setminus Z_1$ variant focuses on semantics related to Z_2 by excluding $\bar{\mathbf{z}}_1$ from the input of $GNN_{\nu}(\cdot)$. In contrast, $M \setminus Z_2$ emphasizes semantics related to Z_1 by excluding $\bar{\mathbf{z}}_2$ from the input of $GNN_{\nu}(\cdot)$. (2) Two variants are created to evaluate the effectiveness of leveraging common and unique relations for OOD generalization. The **M\Comm** variant focuses on unique relations by setting the common relation adjacency matrices A^c as unit diagonal matrices. Conversely, the M\Uniq variant emphasizes common relations by setting A^u as unit diagonal matrices. (3) Two variants are created to study the impact of the latent space model (LSM) and node valuator module. The M\LSM variant

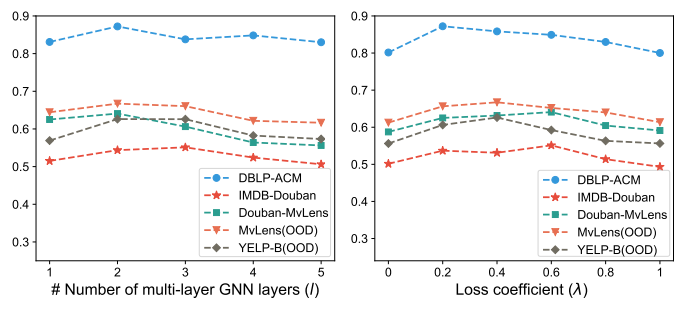


Fig. 6. 2-way 3-shot node classification accuracy of COHF with different parameter settings.

excludes the LSM and does not include structure regularization loss (\mathcal{L}_{str}) when training the model. The **M\Value** variant removes the node valuator module and averages the *K*-shot embedded nodes within a class to derive the class prototype. From Fig. 5, we have the following observations:

- The M\Z₁ and M\Z₂ variants exhibit inferior performance compared to the original COHF. This highlights the importance of the semantics associated with Z₁ and Z₂ in determining node labels.
- The M\Comm and M\Uniq variants are outperformed by COHF, indicating that adopting a relation-level perspective and utilizing common and unique relations is beneficial for identifying features that are resilient to distribution shifts.
- The M\LSM and M\Value variants demonstrate lower performance than COHF, emphasizing the significance of the LSM and valuator modules. The LSM module regularizes model parameters by reconstructing the graph structure, while the valuator module assesses the richness of environment-independent features of nodes in the source HG and evaluates the significance of sparsely labeled nodes in developing robust prototypes for the target HG.

Parameter Study (**RQ3**). We investigate the sensitivity of several important parameters in COHF and illustrate their impacts in Fig. 6. For the number of layers in the multi-layer GNN module, moderate values of 2 or 3 are recommended. This is mainly because meta-paths of lengths 2 and 3 are usually sufficient to capture the necessary semantic information for node classification. Meta-paths longer than these do not typically lead to further performance improvements. For the loss coefficient λ , COHF achieves optimal performance when λ ranges between 0.2 to 0.6. Values of λ that are either too small or too large can lead to degraded performance.

VII. CONCLUSION

In this paper, we introduce a novel problem of OOD generalization in heterogeneous graph few-shot learning, and propose a solution called COHF. Following the invariance principle from causal theory, COHF focuses on invariant factors to address distribution shifts across HGs. Furthermore, COHF incorporates a novel value-based meta-learning framework, which facilitates learning new classes with few-labeled data and varying distributions. Extensive experiments demonstrate the superior performance of COHF. For future work, we plan to explore the application of COHF in other graph learning

tasks, such as link prediction and relation mining, to exploit its potential across a wider range of contexts.

REFERENCES

- C. Shi, Y. Li, J. Zhang, Y. Sun, and S. Y. Philip, "A survey of heterogeneous information network analysis," *IEEE TKDE*, vol. 29, no. 1, pp. 17–37, 2016.
- [2] C. Zhang, K. Ding, J. Li, X. Zhang, Y. Ye, N. V. Chawla, and H. Liu, "Few-shot learning on graphs: A survey," arXiv preprint arXiv:2203.09308, 2022.
- [3] M. Yoon, J. Palowitch, D. Zelle, Z. Hu, R. Salakhutdinov, and B. Perozzi, "Zero-shot transfer learning within a heterogeneous graph via knowledge transfer networks," in NIPS, 2022, pp. 27 347–27 359.
- [4] P. Ding, Y. Wang, and G. Liu, "Cross-heterogeneity graph few-shot learning," in CIKM, 2023, pp. 420–429.
- [5] Z. Zhuang, X. Xiang, S. Huang, and D. Wang, "Hinfshot: A challenge dataset for few-shot node classification in heterogeneous information network," in *ICMR*, 2021, pp. 429–436.
- [6] P. Ding, Y. Wang, G. Liu, and X. Zhou, "Few-shot semantic relation prediction across heterogeneous graphs," *IEEE TKDE*, vol. 35, no. 10, pp. 10265–10280, 2023.
- [7] Q. Zhang, X. Wu, Q. Yang, C. Zhang, and X. Zhang, "Hg-meta: Graph meta-learning over heterogeneous graphs," in SDM, 2022, pp. 397–405.
- [8] Y. Bengio, T. Deleu, N. Rahaman, R. Ke, S. Lachapelle, O. Bilaniuk, A. Goyal, and C. Pal, "A meta-transfer objective for learning to disentangle causal mechanisms," arXiv preprint arXiv:1901.10912, 2019.
- [9] J. Pearl, Causality. Cambridge university press, 2009.
- [10] M. Rojas-Carulla, B. Schölkopf, R. Turner, and J. Peters, "Invariant models for causal transfer learning," *JMLR*, vol. 19, no. 1, pp. 1309– 1342, 2018.
- [11] Y. Lin, H. Dong, H. Wang, and T. Zhang, "Bayesian invariant risk minimization," in CVPR, 2022, pp. 16021–16030.
- [12] Y. Chen, Y. Zhang, Y. Bian, H. Yang, M. Kaili, B. Xie, T. Liu, B. Han, and J. Cheng, "Learning causally invariant representations for out-of-distribution generalization on graphs," NIPS, vol. 35, pp. 22131–22148, 2022.
- [13] S. Fan, X. Wang, Y. Mo, C. Shi, and J. Tang, "Debiasing graph neural networks via learning disentangled causal substructure," *NIPS*, vol. 35, pp. 24 934–24 946, 2022.
- [14] W. Wang, X. Lin, F. Feng, X. He, M. Lin, and T.-S. Chua, "Causal representation learning for out-of-distribution recommendation," in WWW, 2022, pp. 3562–3571.
- [15] C. Finn, P. Abbeel, and S. Levine, "Model-agnostic meta-learning for fast adaptation of deep networks," in *ICML*, 2017, pp. 1126–1135.
- [16] K. Huang and M. Zitnik, "Graph meta learning via local subgraphs," NIPS, vol. 33, pp. 5862–5874, 2020.
- [17] H. Hong, H. Guo, Y. Lin, X. Yang, Z. Li, and J. Ye, "An attention-based graph neural network for heterogeneous structural learning," in AAAI, vol. 34, no. 04, 2020, pp. 4132–4139.
- [18] Q. Lv, M. Ding, Q. Liu, Y. Chen, W. Feng, S. He, C. Zhou, J. Jiang, Y. Dong, and J. Tang, "Are we really making much progress? revisiting, benchmarking and refining heterogeneous graph neural networks," in KDD, 2021, pp. 1150–1160.
- [19] Z. Zhou, J. Shi, R. Yang, Y. Zou, and Q. Li, "Slotgat: slot-based message passing for heterogeneous graphs," in *ICML*, 2023, pp. 42644–42657.
- [20] X. Wang, H. Ji, C. Shi, B. Wang, Y. Ye, P. Cui, and P. S. Yu, "Heterogeneous graph attention network," in WWW, 2019, pp. 2022– 2032.
- [21] X. Fu, J. Zhang, Z. Meng, and I. King, "Magnn: Metapath aggregated graph neural network for heterogeneous graph embedding," in WWW, 2020, pp. 2331–2341.
- [22] S. Yun, M. Jeong, R. Kim, J. Kang, and H. J. Kim, "Graph transformer networks," NIPS, vol. 32, 2019.
- [23] F. Zhou, C. Cao, K. Zhang, G. Trajcevski, T. Zhong, and J. Geng, "Metagnn: On few-shot node classification in graph meta-learning," in CIKM, 2019, pp. 2357–2360.
- [24] Y. Fang, X. Zhao, W. Xiao, and M. de Rijke, "Few-shot learning for heterogeneous information networks," ACM TOIS, 2024.
- [25] Q. Zhang, X. Wu, Q. Yang, C. Zhang, and X. Zhang, "Few-shot heterogeneous graph learning via cross-domain knowledge transfer," in KDD, 2022, pp. 2450–2460.
- [26] A. Baranwal, K. Fountoulakis, and A. Jagannath, "Graph convolution for semi-supervised classification: Improved linear separability and outof-distribution generalization," arXiv preprint arXiv:2102.06966, 2021.

- [27] B. Bevilacqua, Y. Zhou, and B. Ribeiro, "Size-invariant graph representations for graph classification extrapolations," in *ICML*, 2021, pp. 837–851.
- [28] C.-Y. Chuang and S. Jegelka, "Tree mover's distance: Bridging graph metrics and stability of graph neural networks," NIPS, vol. 35, pp. 2944– 2957, 2022.
- [29] D. Krueger, E. Caballero, J.-H. Jacobsen, A. Zhang, J. Binas, D. Zhang, R. Le Priol, and A. Courville, "Out-of-distribution generalization via risk extrapolation (rex)," in *ICML*, 2021, pp. 5815–5826.
- [30] Y.-X. Wu, X. Wang, A. Zhang, X. He, and T.-S. Chua, "Discovering invariant rationales for graph neural networks," arXiv preprint arXiv:2201.12872, 2022.
- [31] Y. Sui, X. Wang, J. Wu, M. Lin, X. He, and T.-S. Chua, "Causal attention for interpretable and generalizable graph classification," in *KDD*, 2022, pp. 1696–1705.
- [32] X. Wang, L. Li, W. Ye, M. Long, and J. Wang, "Transferable attention for domain adaptation," in AAAI, vol. 33, no. 01, 2019, pp. 5345–5352.
- [33] Z. Hao, D. Lv, Z. Li, R. Cai, W. Wen, and B. Xu, "Semi-supervised disentangled framework for transferable named entity recognition," *Neural Networks*, vol. 135, pp. 127–138, 2021.
- [34] M. Wu, S. Pan, C. Zhou, X. Chang, and X. Zhu, "Unsupervised domain adaptive graph convolutional networks," in WWW, 2020, pp. 1457–1467.
- [35] S. Yang, G. Song, Y. Jin, and L. Du, "Domain adaptive classification on heterogeneous information networks," in *IJCAI*, 2021, pp. 1410–1416.
- [36] H. Zhao, R. T. Des Combes, K. Zhang, and G. Gordon, "On learning invariant representations for domain adaptation," in *ICML*, 2019, pp. 7523–7532.
- [37] Y. Sun, J. Han, X. Yan, P. S. Yu, and T. Wu, "Pathsim: Meta path-based top-k similarity search in heterogeneous information networks," *PVLDB*, vol. 4, no. 11, pp. 992–1003, 2011.
- [38] Y. Fang, W. Lin, V. W. Zheng, M. Wu, J. Shi, K. C.-C. Chang, and X.-L. Li, "Metagraph-based learning on heterogeneous graphs," *IEEE TKDE*, vol. 33, no. 1, pp. 154–168, 2019.
- [39] X. Wang, D. Bo, C. Shi, S. Fan, Y. Ye, and S. Y. Philip, "A survey on heterogeneous graph embedding: methods, techniques, applications and sources," *IEEE Transactions on Big Data*, vol. 9, no. 2, pp. 415–436, 2022
- [40] X. Li, D. Ding, B. Kao, Y. Sun, and N. Mamoulis, "Leveraging metapath contexts for classification in heterogeneous information networks," in *ICDE*, 2021, pp. 912–923.
- [41] Y. Yang, Z. Guan, J. Li, W. Zhao, J. Cui, and Q. Wang, "Interpretable and efficient heterogeneous graph convolutional network," *IEEE TKDE*, 2021.
- [42] M. Zhang and Y. Chen, "Link prediction based on graph neural networks," NIPS, vol. 31, 2018.
- [43] J. G. Moreno-Torres, T. Raeder, R. Alaiz-Rodríguez, N. V. Chawla, and F. Herrera, "A unifying view on dataset shift in classification," *Pattern recognition*, vol. 45, no. 1, pp. 521–530, 2012.
- [44] S. Gui, X. Li, L. Wang, and S. Ji, "Good: A graph out-of-distribution benchmark," NIPS, vol. 35, pp. 2059–2073, 2022.
- [45] J. Pearl and D. Mackenzie, The book of why: the new science of cause and effect. Basic books. 2018.
- [46] D. P. Kingma, S. Mohamed, D. Jimenez Rezende, and M. Welling, "Semi-supervised learning with deep generative models," NIPS, vol. 27, 2014
- [47] D. P. Kingma and M. Welling, "Auto-encoding variational bayes," arXiv preprint arXiv:1312.6114, 2013.
- [48] M. Simonovsky and N. Komodakis, "Graphvae: Towards generation of small graphs using variational autoencoders," in *ICANN*, 2018, pp. 412– 422.
- [49] H. Wang, C. Zhou, X. Chen, J. Wu, S. Pan, and J. Wang, "Graph stochastic neural networks for semi-supervised learning," NIPS, vol. 33, pp. 19839–19848, 2020.
- [50] D. M. Blei, A. Kucukelbir, and J. D. McAuliffe, "Variational inference: A review for statisticians," *Journal of the American statistical Association*, vol. 112, no. 518, pp. 859–877, 2017.
- [51] D. Lao, X. Yang, Q. Wu, and J. Yan, "Variational inference for training graph neural networks in low-data regime through joint structure-label estimation," in KDD, 2022, pp. 824–834.
- [52] C. Shi, Y. Lu, L. Hu, Z. Liu, and H. Ma, "Rhine: relation structure-aware heterogeneous information network embedding," *IEEE TKDE*, vol. 34, no. 1, pp. 433–447, 2020.
- [53] T. Chen and Y. Sun, "Task-guided and path-augmented heterogeneous network embedding for author identification," in WSDM, 2017, pp. 295– 304.

- [54] J. Gasteiger, A. Bojchevski, and S. Günnemann, "Predict then propagate: Graph neural networks meet personalized pagerank," arXiv preprint arXiv:1810.05997, 2018.
- [55] A. Vaswani, N. Shazeer, N. Parmar, J. Uszkoreit, L. Jones, A. N. Gomez, Ł. Kaiser, and I. Polosukhin, "Attention is all you need," NIPS, vol. 30, 2017.
- [56] X. Gao, M. Sitharam, and A. E. Roitberg, "Bounds on the jensen gap, and implications for mean-concentrated distributions," arXiv preprint arXiv:1712.05267, 2017.
- [57] T. Wang, J. Huang, H. Zhang, and Q. Sun, "Visual commonsense r-cnn," in CVPR, 2020, pp. 10760–10770.
- [58] S. Abramovich and L.-E. Persson, "Some new estimates of the 'jensen gap'," *Journal of Inequalities and Applications*, vol. 2016, no. 1, pp. 1–9, 2016.
- [59] J. Ma, W. Tang, J. Zhu, and Q. Mei, "A flexible generative framework for graph-based semi-supervised learning," NIPS, vol. 32, 2019.
- [60] P. D. Hoff, A. E. Raftery, and M. S. Handcock, "Latent space approaches to social network analysis," *Journal of the american Statistical associ*ation, vol. 97, no. 460, pp. 1090–1098, 2002.
- [61] K. Ding, J. Wang, J. Li, K. Shu, C. Liu, and H. Liu, "Graph prototypical networks for few-shot learning on attributed networks," in *CIKM*, 2020, pp. 295–304.
- [62] J. Snell, K. Swersky, and R. Zemel, "Prototypical networks for few-shot learning," in NIPS, 2017, pp. 4077–4087.
- [63] B. N. Miller, I. Albert, S. K. Lam, J. A. Konstan, and J. Riedl, "Movielens unplugged: experiences with an occasionally connected recommender system," in *IUI*, 2003, pp. 263–266.
- [64] C. Yang, Y. Xiao, Y. Zhang, Y. Sun, and J. Han, "Heterogeneous network representation learning: A unified framework with survey and benchmark," *IEEE TKDE*, vol. 34, no. 10, pp. 4854–4873, 2020.
- [65] P. Velickovic, G. Cucurull, A. Casanova, A. Romero, P. Lio, Y. Bengio et al., "Graph attention networks," stat, vol. 1050, no. 20, pp. 10–48 550, 2017.
- [66] F. Wu, A. Souza, T. Zhang, C. Fifty, T. Yu, and K. Weinberger, "Simplifying graph convolutional networks," in *ICML*, 2019, pp. 6861–6871.
- [67] K. Xu, W. Hu, J. Leskovec, and S. Jegelka, "How powerful are graph neural networks?" arXiv preprint arXiv:1810.00826, 2018.
- [68] T. N. Kipf and M. Welling, "Semi-supervised classification with graph convolutional networks," arXiv preprint arXiv:1609.02907, 2016.
- [69] W. Hamilton, Z. Ying, and J. Leskovec, "Inductive representation learning on large graphs," in NIPS, 2017, pp. 1025–1035.